Classification of Stratosphere Winter Evolutions Into Four Different Scenarios in the Northern Hemisphere: Part B Coupling With The Surface

Alexis Mariaccia[1], Philippe Keckhut[2], and Alain Hauchecorne[3]

[1]Laboratoire Atmosphères, Milieux, Observations Spatiales (LATMOS)
[2]LATMOS-IPSL
[3]CNRS-IPSL

June 14, 2023

Abstract

We have conducted an investigation into the coupling between the stratosphere and troposphere, focusing on perturbed and unperturbed scenarios of the northern hemisphere polar vortex. These scenarios were established in a previous study, which categorized the main winter typologies based on the timing of sudden stratospheric warmings (SSWs) and final stratospheric warmings (FSWs). Here, we further analyze the mass-weighted divergence of the Eliassen-Palm (EP) flux to confirm the association between these scenarios and the specific timing of momentum and heat flux deposition by planetary waves. Our analysis reveals that wave-1 and wave-2 contributions to this divergence confirm distinct wave activity effects in relation to these scenarios. Additionally, examining the evolutions of the Northern Annular Mode (NAM) provides further insight, demonstrating that these scenarios represent unique states of both the stratosphere and troposphere, which mutually influence each other during the winter months. Of particular interest is the observation of descending stratospheric anomalies into the troposphere following SSWs, often accompanied by a negative phase of the Arctic Oscillation (AO). Notably, we have made an important discovery regarding surface precursors for perturbed scenarios in early winter, specifically December. These surface precursors display wave-like patterns that align with the diagnosed wave activity in the upper stratosphere. This finding establishes a connection between early and late winter, highlighting the importance of these precursors. Consequently, our results enhance our ability to anticipate the behavior of the polar vortex and its impacts, thus holding significant implications for sub-seasonal to seasonal forecasts in the northern hemisphere.

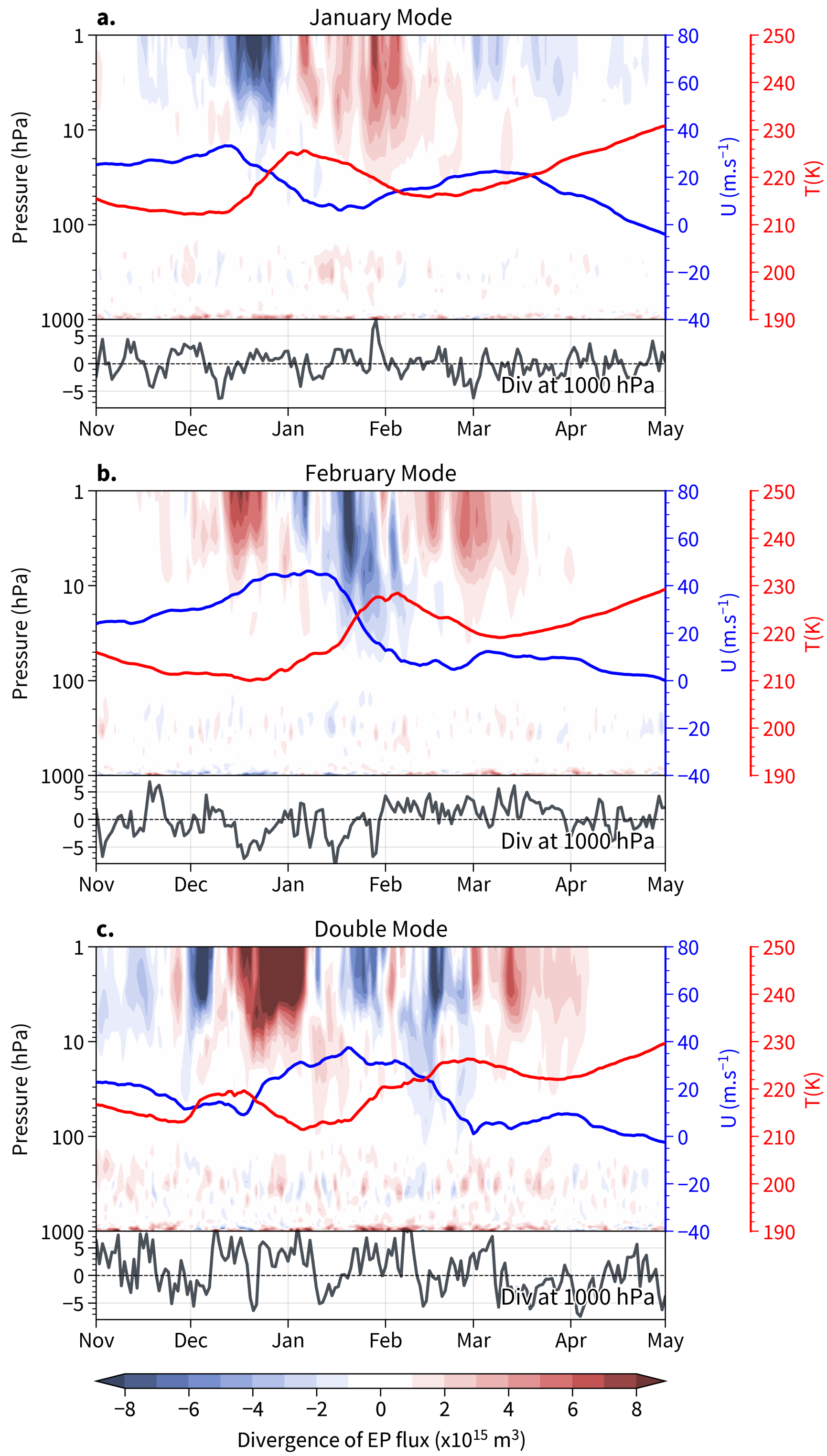
a.
January Mode
b.
February Mode
c.
Double Mode
Pressure (hPa)
U (m.s^{-1})
T(K)
Div at 1000 hPa
Nov
Dec
Jan
Feb
Mar
Apr
May
Divergence of EP flux (x10^{15} m^3)

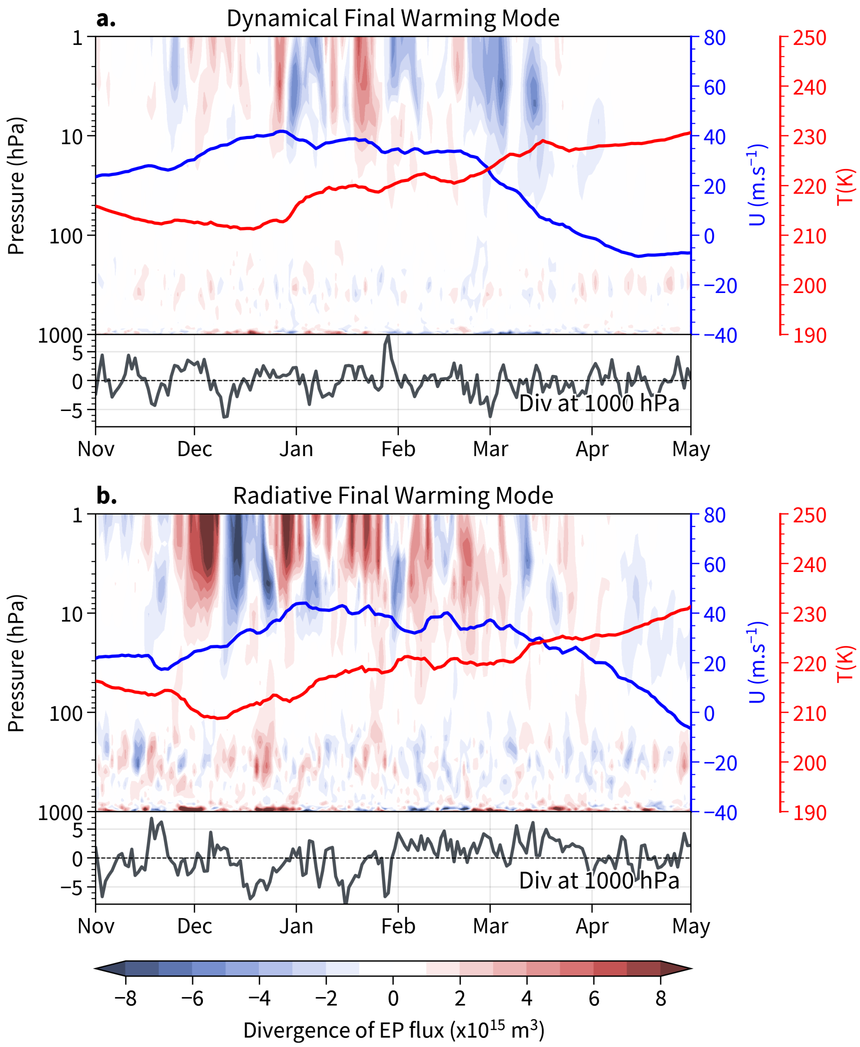
a.
Dynamical Final Warming Mode
b.
Radiative Final Warming Mode
Pressure (hPa)
U (m.s^{-1})
T(K)
Div at 1000 hPa
Nov
Dec
Jan
Feb
Mar
Apr
May
Divergence of EP flux (x10^{15} m^3)

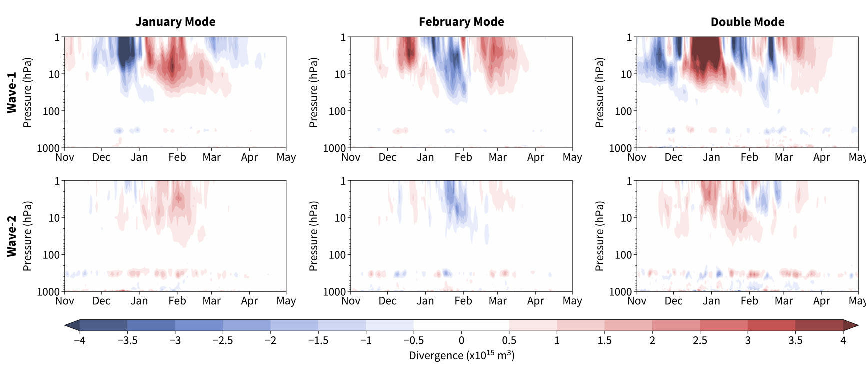
January Mode
February Mode
Double Mode
Wave-1
Wave-2
Pressure (hPa)
Nov
Dec
Jan
Feb
Mar
Apr
May
Divergence (x10^{15} m^3)

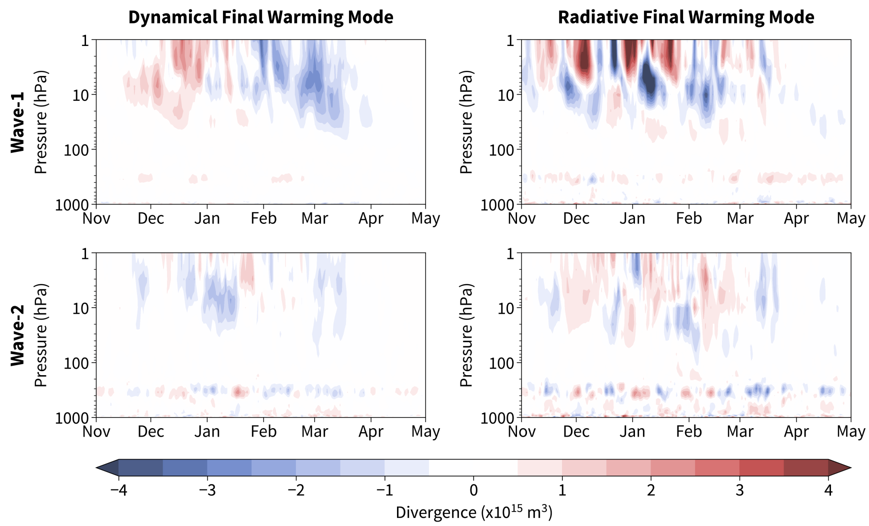

Dynamical Final Warming Mode
Radiative Final Warming Mode
Wave-1
Wave-2
Pressure (hPa)
1
10
100
1000
Nov
Dec
Jan
Feb
Mar
Apr
May
−4
−3
−2
−1
0
1
2
3
4
Divergence (x10^15 m^3)

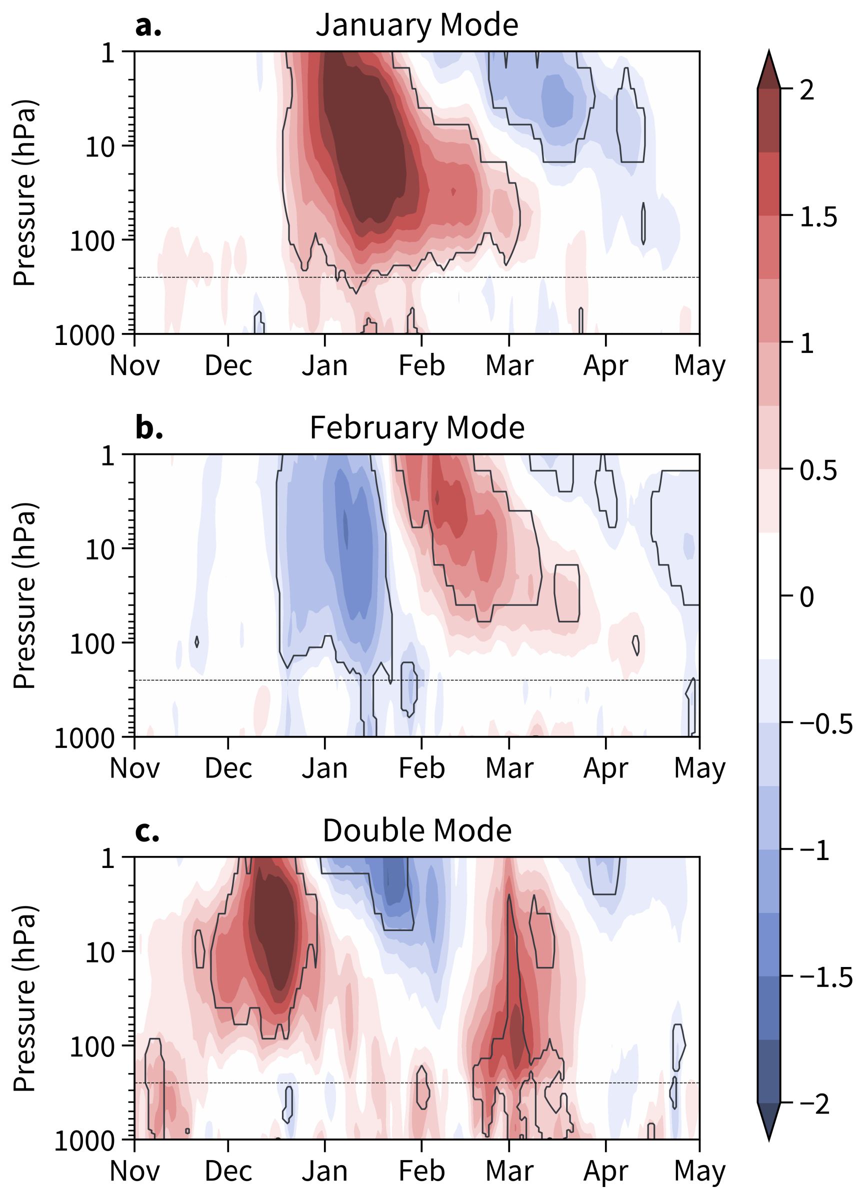
a.
January Mode
b.
February Mode
c.
Double Mode
Pressure (hPa)
1
10
100
1000
Nov
Dec
Jan
Feb
Mar
Apr
May
2
1.5
1
0.5
0
−0.5
−1
−1.5
−2

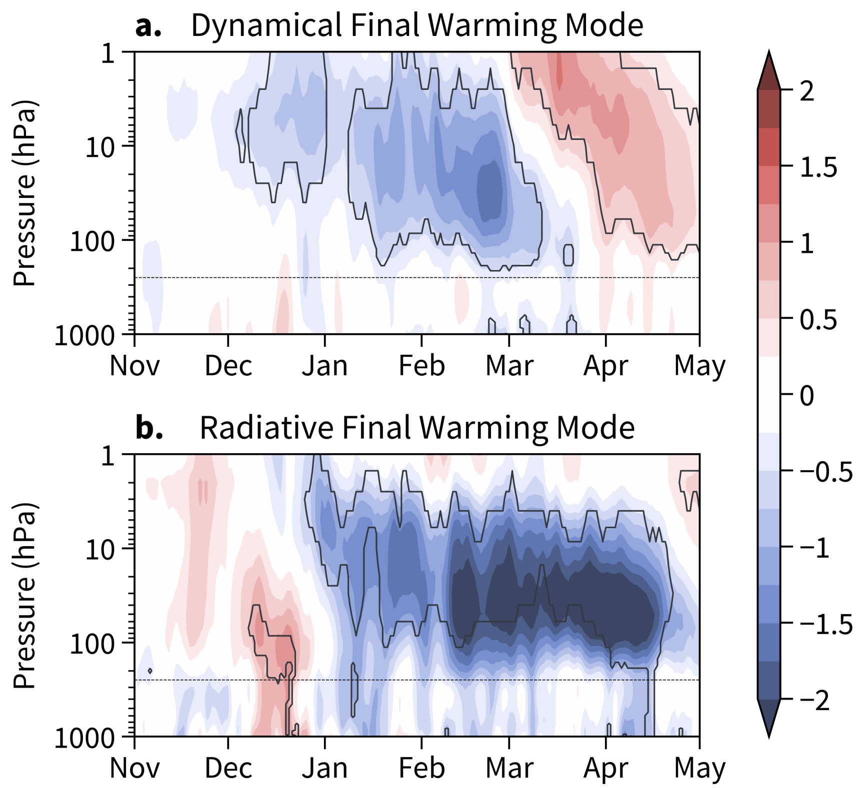
a. Dynamical Final Warming Mode
b. Radiative Final Warming Mode
Pressure (hPa)
1
10
100
1000
Nov
Dec
Jan
Feb
Mar
Apr
May
2
1.5
1
0.5
0
−0.5
−1
−1.5
−2

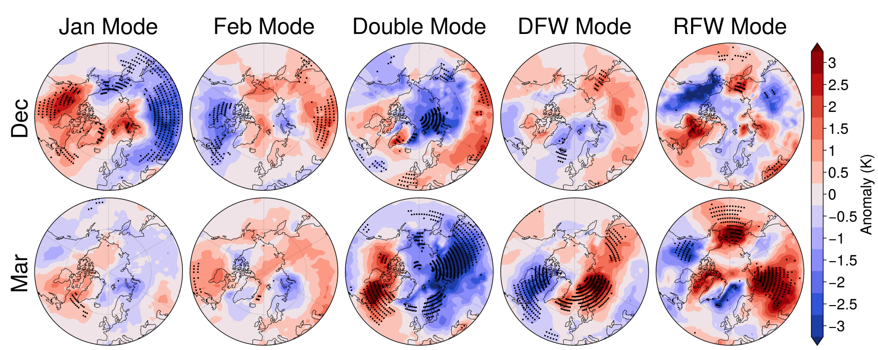
Jan Mode
Feb Mode
Double Mode
DFW Mode
RFW Mode
Dec
Mar
Anomaly (K)
3
2.5
2
1.5
1
0.5
0
−0.5
−1
−1.5
−2
−2.5
−3

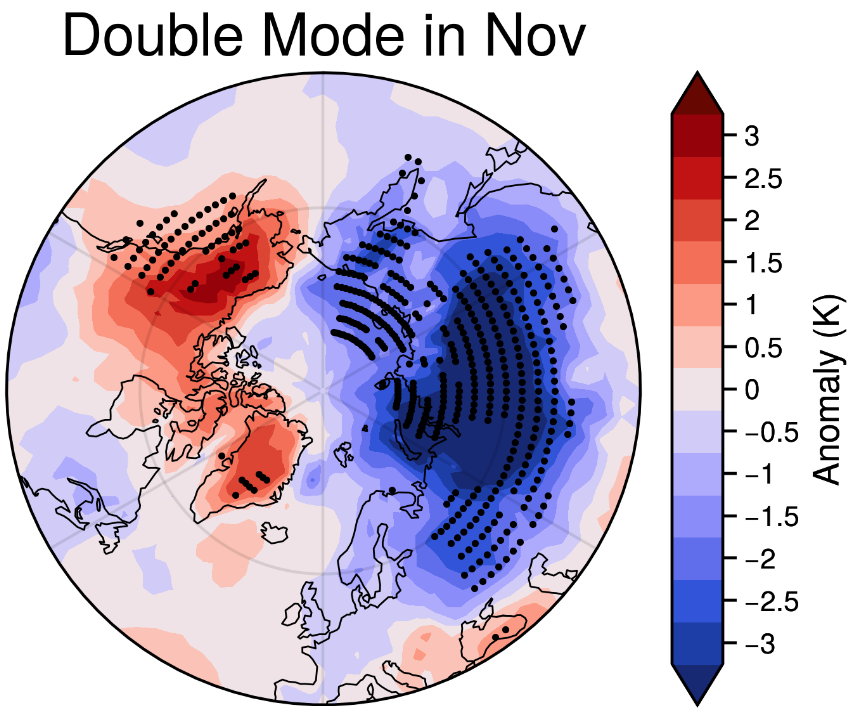
Double Mode in Nov
3
2.5
2
1.5
1
0.5
0
−0.5
−1
−1.5
−2
−2.5
−3
Anomaly (K)

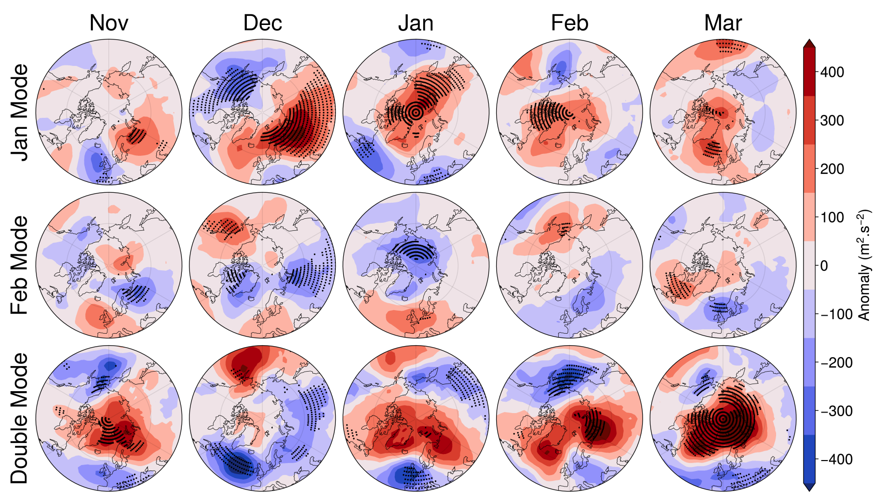
Nov
Dec
Jan
Feb
Mar
Jan Mode
Feb Mode
Double Mode
400
300
200
100
0
-100
-200
-300
-400
Anomaly ($m^2.s^{-2}$)

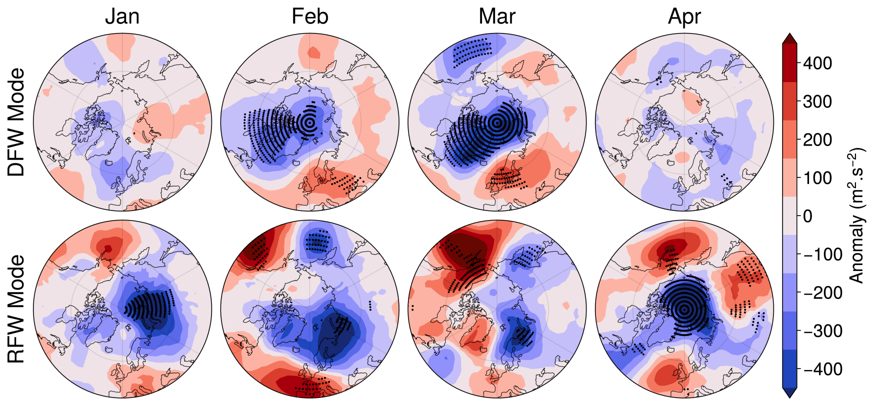
Jan
Feb
Mar
Apr
DFW Mode
RFW Mode
400
300
200
100
0
−100
−200
−300
−400
Anomaly (m².s⁻²)

Classification of Stratosphere Winter Evolutions Into Four Different Scenarios in the Northern Hemisphere: Part B Coupling With The Surface

A. Mariaccia[1], P. Keckhut[1], and A. Hauchecorne[1]

[1]Laboratoire Atmosphères, Milieux, Observations Spatiales, UMR 8190, Institut Pierre-Simon Laplace, Université Versailles-Saint Quentin, Université Paris-Saclay, 78280 Guyancourt, France.

Key Points:

- Distinct wave activity effects are diagnosed for each scenario.
- Each scenario possesses unique stratosphere-troposphere interaction in winter.
- Surface precursors in perturbed scenarios emerge in early winter, especially December.

Corresponding author: Alexis Mariaccia, `alexis.mariaccia@latmos.ipsl.fr`

Abstract

We have conducted an investigation into the coupling between the stratosphere and troposphere, focusing on perturbed and unperturbed scenarios of the northern hemisphere polar vortex. These scenarios were established in a previous study, which categorized the main winter typologies based on the timing of sudden stratospheric warmings (SSWs) and final stratospheric warmings (FSWs). Here, we further analyze the mass-weighted divergence of the Eliassen-Palm (EP) flux to confirm the association between these scenarios and the specific timing of momentum and heat flux deposition by planetary waves. Our analysis reveals that wave-1 and wave-2 contributions to this divergence confirm distinct wave activity effects in relation to these scenarios. Additionally, examining the evolutions of the Northern Annular Mode (NAM) provides further insight, demonstrating that these scenarios represent unique states of both the stratosphere and troposphere, which mutually influence each other during the winter months. Of particular interest is the observation of descending stratospheric anomalies into the troposphere following SSWs, often accompanied by a negative phase of the Arctic Oscillation (AO). Notably, we have made an important discovery regarding surface precursors for perturbed scenarios in early winter, specifically December. These surface precursors display wave-like patterns that align with the diagnosed wave activity in the upper stratosphere. This finding establishes a connection between early and late winter, highlighting the importance of these precursors. Consequently, our results enhance our ability to anticipate the behavior of the polar vortex and its impacts, thus holding significant implications for sub-seasonal to seasonal forecasts in the northern hemisphere.

Plain Language Summary

The stratosphere-troposphere coupling is a dynamic and important area of research, as it is widely recognized that the interactions between the stratosphere and troposphere significantly impact each other, particularly during the winter season. It has been established that accurately representing this coupling in climate models can lead to improvements in weather forecasting. One prominent phenomenon that exemplifies this coupling is sudden stratospheric warming (SSW), which occurs due to interactions between planetary waves and the mean flow in the stratosphere. SSW events can have notable effects on the surface, including potential shifts in extra-tropical storm tracks and the occurrence of severe cold-air outbreaks. Given the significant impacts of SSWs, the scientific community has been actively working towards classifying these events based on their characteristics and impacts. In a previous study, a novel classification scheme was introduced, which identified four distinct scenarios for the northern hemisphere polar vortex based on the timings of SSWs and final stratospheric warmings (FSWs). In this paper, we aim to evaluate the stratosphere-troposphere coupling for each of these scenarios during the winter months, with the goal of identifying potential associated precursors.

1 Introduction

The understanding of stratosphere-troposphere coupling is a crucial aspect of improving seasonal weather predictions in atmospheric sciences. This field of research has gained significant attention due to its impact on the mutual influence between the stratospheric polar vortex and the tropospheric circulation during the northern hemisphere winter. One of the key models, developed by Matsuno (1970), explains that variations in the strength of the wintertime stratospheric circulation are a result of the interaction between the mean flow and upward propagating planetary waves that transport westward momentum from the troposphere. These interactions can give rise to sudden stratospheric warming (SSW) events, characterized by increased polar cap temperatures, weakened polar vortex, and even the reversal of westerly winds in extreme cases. The subsequent stratospheric circulation anomalies can descend into the troposphere, influencing surface weather patterns for up to two months. Additionally, equatorial stratospheric cooling can also occur as a result of these events. Mechanisms responsible for the downward propagation of stratospheric anomalies have been summarized in previous studies by Tripathi et al. (2015) and Kidston et al. (2015).

The northern hemisphere annular mode (NAM) is a commonly used measure for assessing stratosphere-troposphere coupling during SSW events. Baldwin and Dunkerton (2001), for example, computed NAM indices from weak and strong vortex composites and observed that these events are often followed by the Arctic Oscillation (AO) pattern at the surface, which can persist for up to two months. The stratospheric anomaly propagating downward has numerous consequences for tropospheric weather, including shifts in storm track locations, changes in the likelihood and intensity of mid-latitude storms, variations in the frequency of high-latitude blocking events, and the occurrence of cold air outbreaks across the hemisphere (Thompson & Wallace, 2001). However, it is worth noting that not all SSW events result in a systematic tropospheric response, and the same is true for final stratospheric warming (FSW) events (Butler & Domeisen, 2021). Therefore, there has been ongoing research in the scientific community to classify SSW and FSW events and understand the factors that determine their different impacts on tropospheric circulation.

Traditionally, extreme SSW events have been classified as major based on the reversal of westerly winds at 10hPa-60°N (Butler et al., 2015). However, this criterion alone does not indicate whether an SSW event propagates downward. Other studies have classified SSW events based on the geometry of the polar vortex, distinguishing between displaced and splitting types (Charlton & Polvani, 2007; Cohen & Jones, 2011; Mitchell et al., 2013). Mitchell et al. (2013) found that splitting types tend to propagate downward, although this trend was not consistently observed in the study by Charlton and Polvani (2007), and exceptions exist, such as the SSW events observed in the winter of 1998/1999 (Baldwin & Dunkerton, 2001). Nevertheless, this finding aligns with the observations of Nakagawa and Yamazaki (2006), as displacement and splitting types are generally associated with upward fluxes of wavenumbers 1 and 2, respectively. However, the role of wave-1 activity is also significant in the occurrence of SSW events (Nakagawa & Yamazaki, 2006; Bancalá et al., 2012; Barriopedro & Calvo, 2014), and similar downward impacts can occur after both wave-1 and wave-2 SSW events, as seen in the SSWs of January 2009 (wave-2 type) and January 2010 (wave-1 type) (Ayarzagüena et al., 2011; Kodera et al., 2015).

While some studies have directly classified SSWs based on their tropospheric responses, such as absorbing or reflecting types (Kodera et al., 2016), the persistence of stratospheric anomalies (Runde et al., 2016), or surface observations of the North Atlantic Oscillation (Domeisen, 2019)and North Atlantic storm track response (Afargan-Gerstman & Domeisen, 2020), there are significant dissimilarities between these classifications in terms of identifying which SSW events have a descending effect (Karpechko et al., 2017) (see Table 1). Furthermore, Runde et al. (2016) found that 20% of extreme stratospheric events, including both strong and weak vortex events, resulted in a surface response, indicating that the mechanism responsible for the descending effect is still unclear, although anomalies in the lower stratosphere seem to play a crucial role.

On the other hand, FSW events have been classified based on their timing and nature, distinguishing between "early" and "dynamical" or "late" and "radiative" events (Waugh & Rong, 2002; Hauchecorne et al., 2022). The occurrence mechanism between mid-SSWs and early dynamical FSWs, both driven by waves, is similar (Vargin et al., 2020). Butler and Domeisen (2021) classified FSW events in both the northern and southern hemispheres based on dominant zonal wavenumber, timings, and their respective downward impacts. Interestingly, in the northern hemisphere, wave-2 events are followed by anomalously positive 500 hPa height anomalies over the North Pacific and the U.S., in contrast to wave-1 events, although the negative AO pattern remains consistent.

Recently, Mariaccia, Keckhut, and Hauchecorne (2022) proposed a new classification based on empirical orthogonal functions of stratospheric zonal wind fluctuation patterns at the edge of the polar vortex. Their study revealed four scenarios modulated by the timings and dynamical activities of important SSWs (ISSWs) occurring in mid-winter, along with scenarios without ISSWs but differing in the type of FSW (dynamical and early or radiative and late). This novel classification focuses on the entire winter evolution rather than specific SSW or FSW events, and it establishes a connection between mid-winter and winter end, highlighting the existence of a stratospheric memory as previously highlighted by Hauchecorne et al. (2022).

The primary objectives of this study are twofold: first, to demonstrate that this classification represents not only the unfolding of wintertime stratospheric circulation at the edge of the polar vortex but also the overall influence of northern hemisphere stratospheric evolutions on the troposphere during winter, and second, to investigate how stratospheric anomalies descend into the troposphere and manifest as surface signals throughout the winter season in the northern hemisphere. Additionally, the study aims to identify potential precursors at the surface in the months leading up to significant stratospheric anomalies, which could provide insights for seasonal predictability.

The structure of the paper is organized as follows. Section 2 presents the data extraction process from the ERA5 product, as well as the methods used to compute the NAM indices and the divergence of Eliassen-Palm flux in the stratosphere-troposphere. Section 3 describes the four scenarios and their respective dynamical characteristics. Sections 4 and 5 provide an analysis of NAM evolutions and surface impacts for the perturbed and unperturbed scenarios. Then, the impacts on surface temperature in early and late winter are examined in Section 6. Finally, Section 7 presents the summary and conclusions of the study, along with a discussion of its implications for seasonal predictability and future research directions.

2 Data and Method

2.1 ERA5 reanalysis

Since 2016, the European Centre for Medium-Range Weather Forecasts (ECMWF) has been generating a state-of-the-art reanalysis dataset called ERA5. This new generation of reanalysis benefits from the updated ECMWF Integrated Forecast System Cycle 41r2, which incorporates improved model parameterizations of convection and microphysics (Hersbach et al., 2020). ERA5 provides hourly output on a 0.25° latitude-longitude grid, with 137 vertical levels extending from the surface up to a pressure level of 0.01 hPa (approximately 80 km). As a result, ERA5 offers the longest reanalysis series available, spanning from 1940 to the present.

Recent studies have demonstrated that ERA5 temperature reanalysis accurately reproduces observed temperatures and their variability within the upper stratosphere during winter (Marlton et al., 2021; Mariaccia, Keckhut, Hauchecorne, Claud, et al., 2022). However, the mesosphere is not as well represented in ERA5. Consequently, the ERA5 dataset is particularly suitable for studying stratosphere-troposphere coupling over decades, specifically during the winter season.

ERA5 data is also readily available at 37 pressure levels, covering the entire troposphere-stratosphere region from 1000 to 1 hPa, with 11 additional levels between 100 and 1 hPa. For our analysis, we extracted the daily variables required to compute the Northern Annular Mode (NAM) indices and Eliassen-Palm flux from ERA5 reanalysis data at these pressure levels. Our analysis covers the grid from 20°N poleward and spans from 1950 to 2020, encompassing a total of 70 winters. The winter season in our analysis starts on November 1st and concludes on May 1st, spanning a period of 182 days.

2.2 Calculating the NAM indices

The Northern Annular Mode (NAM), also known as the North Atlantic Oscillation, is a key measure of dynamic variability during the winter season. It is computed by determining the leading empirical orthogonal function (EOF) that captures the dominant patterns of variability. The computation of NAM indices enables us to assess the influence of stratospheric variability on the spatial patterns observed in the troposphere.

Several methods exist for computing NAM indices, including surface-based EOFs, height-dependent EOFs, and zonal-mean EOFs. Each method has its advantages and drawbacks. The first two methods have limitations in capturing realistic annular variability in the middle atmosphere, as well as computational costs. In contrast, the zonal-mean EOFs method, as described by Baldwin and Thompson (2009), based on daily averaged, zonally averaged, year-round geopotential height, consistently captures annular variability structures and is employed in this study.

To calculate the daily NAM indices (y_l^d), the following equation is used:

$$y_l^d = \frac{\overline{Z_l^d} W e_l}{(e_l)^T W e_l}, \tag{1}$$

where $\bar{Z_l^d}$ represents the zonal mean of the daily geopotential anomaly, W is a vector used to spatially weight the NAM indices (cosine of latitudes), and e_l denotes the leading EOF of all zonal mean daily geopotential anomalies. Thus, we computed NAM indices for the 70 winters spanning from 1950 to 2020 using Equation 1. Subsequently, we averaged the daily NAM indices over the winters associated with each mode to obtain the mean time-height development of the northern annular mode.

By applying this approach, we can analyze the behavior of the NAM and its link to stratospheric variability, providing valuable insights into the stratosphere-troposphere coupling over the winter season.

2.3 Student's t-test

To assess the significance of the mean NAM indices and anomalies at 1000 hPa for each scenario, Student's t-tests were conducted. For the mean NAM indices, the null hypothesis of the t-test states that the means of the datasets are equal to the mean NAM indices observed over the 70 winters. On the other hand, for anomalies at 1000 hPa, the null hypothesis assumes that the means of the datasets are equal to zero. By performing these t-tests, we can determine whether the observed differences in the mean NAM indices and anomalies are statistically significant.

2.4 The divergence of Eliassen-Palm flux

The Eliassen-Palm (EP) flux is a vector that characterizes the direction of small atmospheric waves as well as the magnitude of eddy heat flux and momentum flux. It serves as a valuable diagnostic tool for investigating wave-mean flow interactions and, consequently, the coupling between the stratosphere and troposphere. The divergence of the EP flux provides information about the acceleration or deceleration of the zonal mean zonal wind.

In this study, ERA5 data has been extracted onto pressure levels and latitude degrees, and the divergence of the EP flux is computed using the methodology described by Jucker (2021). This approach accounts for spherical geometry, the aspect ratio of the figures, and the units of the vector components. The components of the EP flux in pressure coordinates are calculated using the equations introduced by Andrews et al. (1983):

$$f_\phi = -\overline{u'v'} + \overline{u}_p \frac{\overline{v'\theta'}}{\bar{\theta}_p}, \tag{2}$$

$$f_p = \left(f - \frac{1}{a\cos\phi} \frac{\partial(\bar{u}\cos\phi)}{\partial\phi} \right) \frac{\overline{v'\theta'}}{\bar{\theta}_p} - \overline{u'\omega'}, \tag{3}$$

where the notation follows the conventional usage, and primes and overbars represent perturbations and zonal means, respectively. Subscripts ϕ and p refer to partial derivatives with respect to latitudes and pressure levels. f denotes the Coriolis parameter, and a represents the radius of the Earth. The unit of f_ϕ is $\mathrm{m}^2/\mathrm{s}^2$, and assuming pressure is in hPa, f_p is in $\mathrm{m} \cdot \mathrm{hPa}/\mathrm{s}^2$. To obtain the natural form of divergence on the (ϕ, p) plane, it is necessary to express the EP flux components in the scale units for ϕ and p on the diagram, as outlined by Edmon et al. (1980):

$$\mathbf{F} = \left(\hat{F}_\phi, \hat{F}_p\right) = \frac{2\pi}{g} a^2 \cos^2\phi \left(f_\phi, a f_p\right). \tag{4}$$

where $\mathbf{F}$ represents the EP flux components in the desired scale units. Finally, the mass-weighted divergence of $\mathbf{F}$ is simply given by $\partial_\phi \hat{F}_\phi + \partial_p \hat{F}_p$ and is expressed in units of m^3. In this study, the anomaly of EP flux divergence is computed daily for each winter on all pressure levels throughout the analyzed period. The mean divergence anomalies associated with the four different scenarios are presented in the subsequent section. The contributions of wave-1 and wave-2 to the mean divergence anomaly for each scenario are also calculated and can be found in the appendix section. However, a detailed discussion of their contributions will be provided in the following section.

3 The Dynamics of the Four Vortex Scenarios

A recent study by Mariaccia, Keckhut, and Hauchecorne (2022) classified 61 out of the 70 winters between 1950 and 2020 into four scenarios representing typical polar vortex evolutions. These scenarios include the January mode (17 winters), the February mode (17 winters), the Double mode (seven winters), and the unperturbed polar vortex evolution consisting of the Dynamical Final Warming (DFW) mode (15 winters) and the Radiative Final Warming (RFW) mode (five winters). The complete list of winters associated with each scenario can be found in Mariaccia, Keckhut, and Hauchecorne (2022). For the remainder of this study, we will focus separately on the DFW and RFW modes. Mariaccia, Keckhut, and Hauchecorne (2022) also found that each scenario exhibits distinct wave-1 and wave-2 activities in the middle stratosphere, consistent with zonal wind patterns over the winter months. However, as this investigation focused on a specific point in the northern hemisphere stratosphere (10 hPa and 60°N), further analysis is needed to confirm these trends at other altitudes and latitudes near the polar vortex edge.

To better understand the interaction between waves and the mean flow, we calculated the mean mass-weighted divergence anomaly of Eliassen-Palm flux for winters associated with perturbed and unperturbed scenarios. Figures 1 and 2 in this study show the divergence anomalies for perturbed and unperturbed scenarios, respectively. The wave-1 and wave-2 contributions to this divergence are provided in the appendix (Figures A1 and A2). We also examined the zonal mean zonal wind and temperature evolutions between 50°N and 70°N at 10 hPa to assess the effects of the EP flux divergence. These zonal mean evolutions closely resemble those reported by Mariaccia, Keckhut, and Hauchecorne (2022) at 60°N-10 hPa, confirming that the typologies identified in the northern hemisphere stratosphere are widespread.

In terms of the divergence patterns, significant signals are primarily observed in the upper stratosphere, where planetary waves break and deposit their momentum. As expected, we find that negative (positive) divergence values align with the deceleration (acceleration) of zonal winds and temperature increase (decrease) associated with SSWs and FSWs (polar vortex reinforcements). These results confirm the role of wave-mean flow interactions in weakening the zonal stratospheric circulation and warming the stratosphere. The magnitude and vertical extension of the divergence signal are likely responsible for the abrupt zonal wind deceleration observed at 10 hPa, with the February mode exhibiting a stronger wind deceleration gradient due to a negative divergence signal extending into the lower stratosphere. Interestingly, the divergence anomaly evolutions at 1000 hPa tend to herald the current or future signs of those in the upper stratosphere. These signals constitute a first attestation of the probable existent influences on the stratospheric dynamics by the surface climate.

In contrast, the divergences associated with the DFW and RFW modes display frequent oscillations between positive and negative values in the upper stratosphere over winter. These oscillations, accompanied by momentum and heat flux depositions on short time scales, are likely the reasons why winters in these modes remain unperturbed. Thus, it appears that longer periods of wave-mean flow interactions generating momentum and heat flux, as observed in the perturbed scenarios, are necessary to have a significant impact on the stratospheric circulation.

The contributions of wave-1 and wave-2 to the divergence evolutions align with the wave activity analysis performed by Mariaccia, Keckhut, and Hauchecorne (2022) for each scenario. The January and Double modes are predominantly driven by wave-1, while the February mode exhibits contributions from both wave-1 and wave-2. However, an interesting exception is observed in the DFW mode in December, where wave-1 accelerates the mean flow while wave-2 decelerates it. In the perturbed modes, wave-2 activity only influences the acceleration of the mean flow in the January and Double modes, whereas the opposite is true for the February mode.

These new findings further support the previously reported dynamical behaviors and enhance our understanding of wave activities in different scenarios and their impacts on polar vortex evolutions. However, since the mean divergence anomaly signals are primarily located in the upper stratosphere, it is challenging to infer how momentum and heat flux anomalies affect the troposphere. Therefore, in the next section, we investigate the troposphere-stratosphere coupling by examining the NAM evolutions for each scenario.

4 Perturbed Vortex Scenarios

4.1 NAM evolutions

Figure 3 illustrates the mean time-height evolution of the NAM indices calculated in the troposphere and stratosphere for the three perturbed scenarios: January, February, and Double modes. The figure includes solid black contour lines to indicate significant anomalies based on the Student's t-test. Weak and warm polar vortex periods are depicted in red, while strong and cold polar vortex periods are shown in blue. These findings align with previous studies, which have established that anomalies in the stratosphere exhibit longer time scales compared to fluctuations in the troposphere. Additionally, anomalies tend to first appear in the upper stratosphere before descending downward (Baldwin & Dunkerton, 2001; Mitchell et al., 2013). Furthermore, anomalies reaching the lower stratosphere tend to persist longer than those in the upper stratosphere due to the extended radiative time scale. Notably, strong anomalies located just above the tropopause have a higher tendency to propagate into the troposphere, underscoring the significance of this factor in the downward mechanism. Importantly, these NAM evolutions are consistent with the divergence evolutions of EP flux for the perturbed scenarios (see Figure 1).

For the January mode, an instantaneous and significant positive anomaly associated with weak polar vortex events caused by an ISSW emerges at the end of December. This

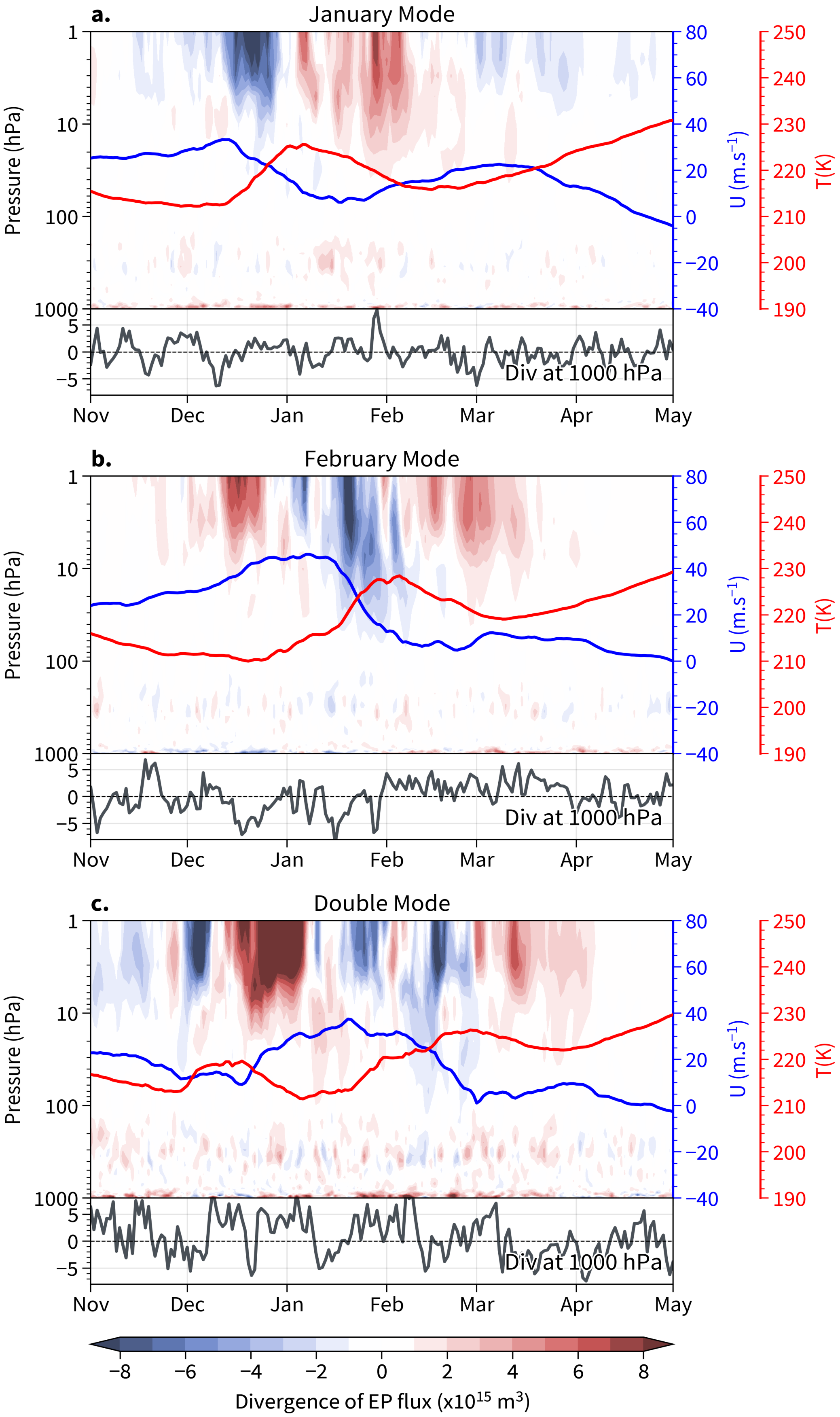

Figure 1. Mean time-height development of the anomaly of the mass-weighted divergence of Eliassen-Palm flux between 50 and 70°N for the three perturbed scenarios: the January Mode (a), the February Mode (b), and the Double Mode (c). Shaded negative (blue) and positive (red) values correspond to a deceleration and acceleration of the zonal wind, respectively. The panel at the bottom shows the evolution at 1000 hPa. Solid blue and red lines represent mean evolution of zonal mean zonal wind and zonal mean temperature, respectively, computed over the latitude range 50-70°N at 10 hPa.

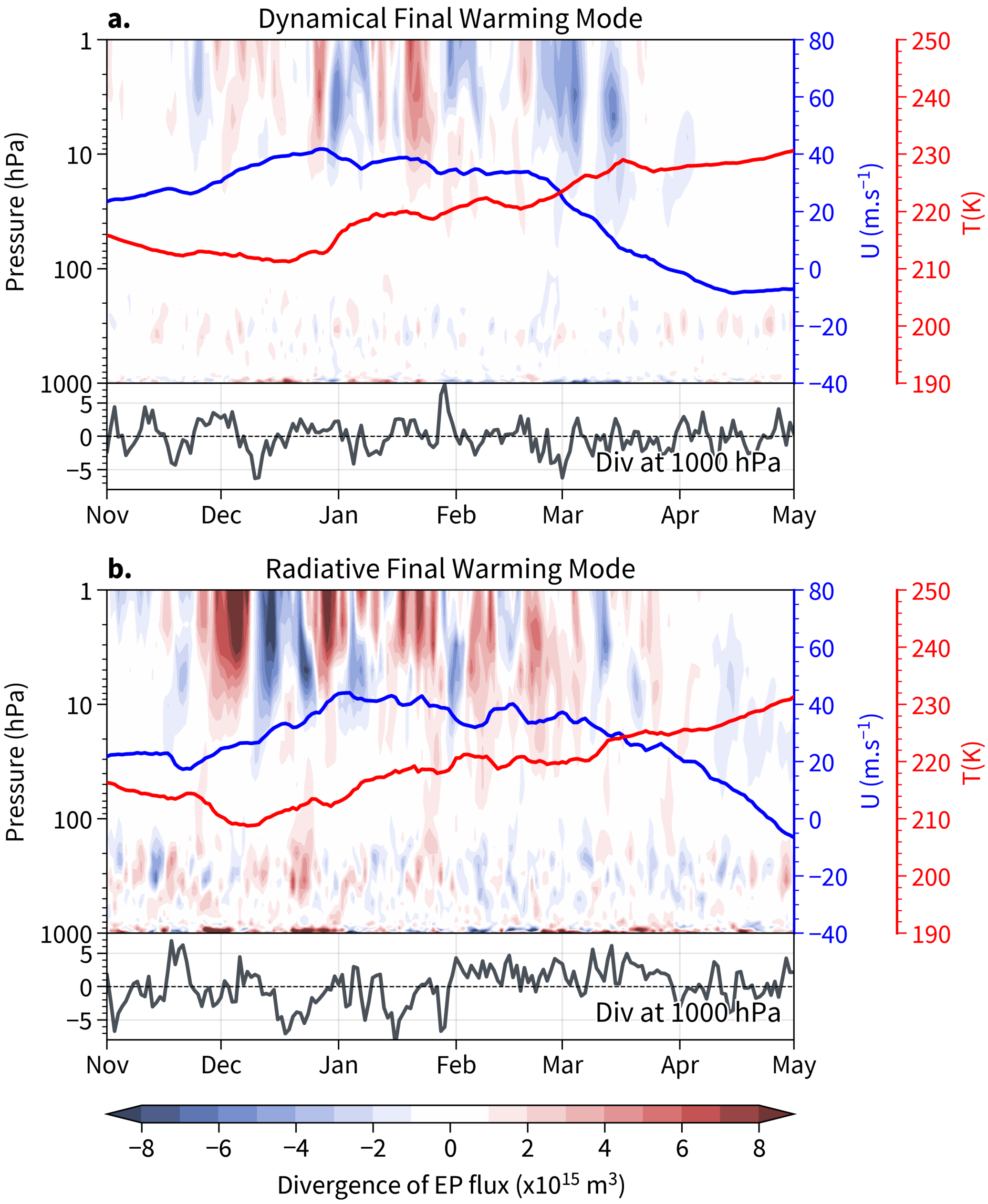

Figure 2. Mean time-height development of the anomaly of the mass-weighted divergence of Eliassen-Palm flux between 50 and 70°N for the two sub-modes composing the unperturbed scenario: the Dynamical Final Warming Mode (a) and the Radiative Final Warming Mode (b). Shaded negative (blue) and positive (red) values correspond to a deceleration and acceleration of the zonal wind, respectively. The panel at the bottom shows the evolution at 1000 hPa. Solid blue and red lines represent mean evolution of zonal mean zonal wind and zonal mean temperature, respectively, computed over the latitude range 50-70°N at 10 hPa.

anomaly rapidly propagates throughout the stratosphere with high significance from December to January. It covers the entire stratosphere and subsequently moves downward into the troposphere, reaching the Earth's surface significantly in January. From February, the positive anomaly begins descending from the upper to lower stratosphere, with a slight rise from the tropopause, halting the propagation into the troposphere. Another noteworthy positive anomaly at the surface emerges in late March, potentially representing a late tropospheric response to the strong positive anomaly that concluded in March. Simultaneously, a weak negative anomaly appears in the upper stratosphere, propagating downward to reach the lower stratosphere in April, without extending into the troposphere. The FSW, which commonly occurs around April 20th (Mariaccia, Keckhut, & Hauchecorne, 2022), does not induce a strong signal in the stratosphere or troposphere. Thus, these results align with the typical winter evolutions associated with this scenario, characterized by ISSWs in mid-January, followed by a weak reinforcement of the polar vortex in March before concluding in April. It is worth noting that, on average, no stratospheric anomaly precedes the positive anomaly associated with the ISSW's appearance at the end of December. This absence of an anomaly is attributable to the similarity in the seasonal wave activity cycle up to mid-December for most winters (Mariaccia, Keckhut, & Hauchecorne, 2022), resulting in a zero anomaly in the stratosphere at the beginning of winter. Beyond mid-December, the mean wave activity associated with the scenarios begins to diverge.

In the case of the February mode, a significant negative anomaly indicating strong polar vortex events instantaneously emerges and covers the entire stratosphere from mid-December to the end of January. Importantly, as this anomaly descends further toward the tropopause, it begins to significantly impact the troposphere, confirming the importance of this factor once again. Subsequently, a positive anomaly primarily appears in the upper stratosphere at the end of January, with a tilted descending phase that later reaches the lower stratosphere, lasting until April. However, no significant descent into the troposphere is observed since the positive anomaly remains predominantly above 100 hPa, which is too high to affect the tropopause and enable downward propagation. Nevertheless, positive anomaly signals, albeit not significant, emerge at the surface in March, suggesting a weak tropospheric response to this stratospheric anomaly on average. From March onward, a weak negative anomaly signal develops in the upper stratosphere, descending to the lower stratosphere, indicating the final formation of the polar vortex with weak winds before the occurrence of the FSW, often characterized by late and radiative events. Similar to the January mode, no significant anomaly precedes the negative anomaly in December in the stratosphere, as explained earlier. Therefore, these findings align with the mean zonal evolution associated with the February mode, featuring a stratospheric circulation reinforcement in December and January, followed by a rapid zonal wind deceleration due to an ISSW occurring at the end of January, before a radiative FSW at the end of April.

Lastly, winters associated with the Double mode exhibit, on average, a positive anomaly in the troposphere from mid-November. Surprisingly, unlike the January and February modes, this anomaly appears to propagate upward from the surface and precedes another positive anomaly covering the entire stratosphere from mid-December, corresponding to the first ISSW's occurrence. This upward propagation suggests that the positive anomaly at the surface acts as a tropospheric precursor to the subsequent ISSW's appearance. Hence, this anomaly propagation exemplifies the bidirectional stratospheric-tropospheric dynamical coupling and its potential usefulness for seasonal-scale climate forecasts. The positive anomaly descends into the lower stratosphere and propagates into the troposphere from mid-January. Concurrently, a negative anomaly emerges in the upper stratosphere from the beginning of January, descending to the lower stratosphere by early February, indicating the reformation of the polar vortex. Starting from mid-February, a new positive anomaly emerges, covering both the stratosphere and troposphere until the end of March. Interestingly, the maximum positive anomaly is observed at low altitudes around 200 hPa, corresponding to the second ISSW's occurrence. Thus, similar to the previous two modes, these findings align with the unfolding of mean stratospheric winter circulation and wave activity for the Double mode (see Figure 1), featuring an initial ISSW in December, a subsequent one around the end of February, and a vortex restoration between the two. In April, a negative anomaly begins to develop in the upper stratosphere, corresponding to a tentative restoration of the polar vortex, which is interrupted by the FSW, often characterized by late and radiative events during this period. The absence of propagation of this negative anomaly suggests that the presence of tropospheric anomalies is unrelated.

In conclusion, these mean time-height evolutions of NAM indices indicate that these three perturbed scenarios possess distinct vertical structures influenced by the timings of ISSWs and FSWs. On the whole, positive anomalies generated by ISSWs tend to propagate downward into the troposphere immediately or with a delay of one month after their occurrence. However, this behavior is not observed for FSWs, which are mostly radiative and do not tend to impact the troposphere significantly. Notably, both the stratosphere and troposphere exhibit weak signals in April. These findings affirm that the new classification determined in Mariaccia, Keckhut, and Hauchecorne (2022) not only represents different stratospheric wind scenarios but also repetitive typical spatial patterns that couple the stratosphere with the troposphere during Northern Hemisphere winters. In the next section, we will discuss the probable polar vortex geometry associated with these perturbed scenarios by comparing with the classification performed in Mitchell et al. (2013). Then, we will investigate the surface regions impacted in the Northern Hemisphere over the months for these three perturbed scenarios.

4.2 Link With Horizontal Polar Vortex Geometry

The propagation of instantaneous anomalies throughout the stratosphere and troposphere after ISSWs in the January mode bears resemblance to the findings of Splitting events in Mitchell et al. (2013) (see Figure 4b), suggesting a potential wave resonance phenomenon caused by barotropic mode excitation (Esler & Scott, 2005). Thus, one might expect the January mode to be associated with splitting polar vortex evolutions. However, this concurrence is surprising since the January mode is primarily driven by wave-1 activity, usually characterized by displaced events. Similarly unexpected, the tilted downward propagation observed in the stratosphere for the February mode aligns with the findings for Displacement events in Mitchell et al. (2013) (see Figure 4a), showing limited impacts in the troposphere. This result is also surprising as the February mode exhibits strong wave-2 activity, typically associated with splitting events. Moreover, this result is consistent with the seasonal distribution of splitting, displacement, and mixed events presented in Mitchell et al. (2013) (see Figure 3), where splitting events are more concentrated in December and January, while displaced events occur more frequently in February and March. However, it should be noted that this distribution differs from that obtained by Charlton and Polvani (2007), who used a different method to identify polar vortex geometry during SSWs. This discrepancy highlights the importance of considering methodological uncertainties when comparing these classifications. Hence, despite these seemingly contradictory findings, all inferences drawn from this comparison are likely irrelevant. The primary reason is that the established scenarios are not based on specific SSW dates but rather on winter typologies, representing a novel approach that hampers direct comparisons with such classifications. Furthermore, even previous SSW classifications exhibit contradictions and divergences in identifying the mechanism responsible for downward effects into the troposphere (Karpechko et al., 2017), necessitating further clarification. Additionally, most studies, including the NAM evolutions presented here, argue that the persistence of circulation anomalies in the lower stratosphere plays a crucial role in this process. Consequently, without making assumptions with significant uncertainties, it is impossible to draw conclusions regarding the vortex geometry associated with these perturbed scenarios. Nonetheless, this feature appears to be less decisive than the timing of ISSWs in predicting stratospheric anomaly descents and surface impacts.

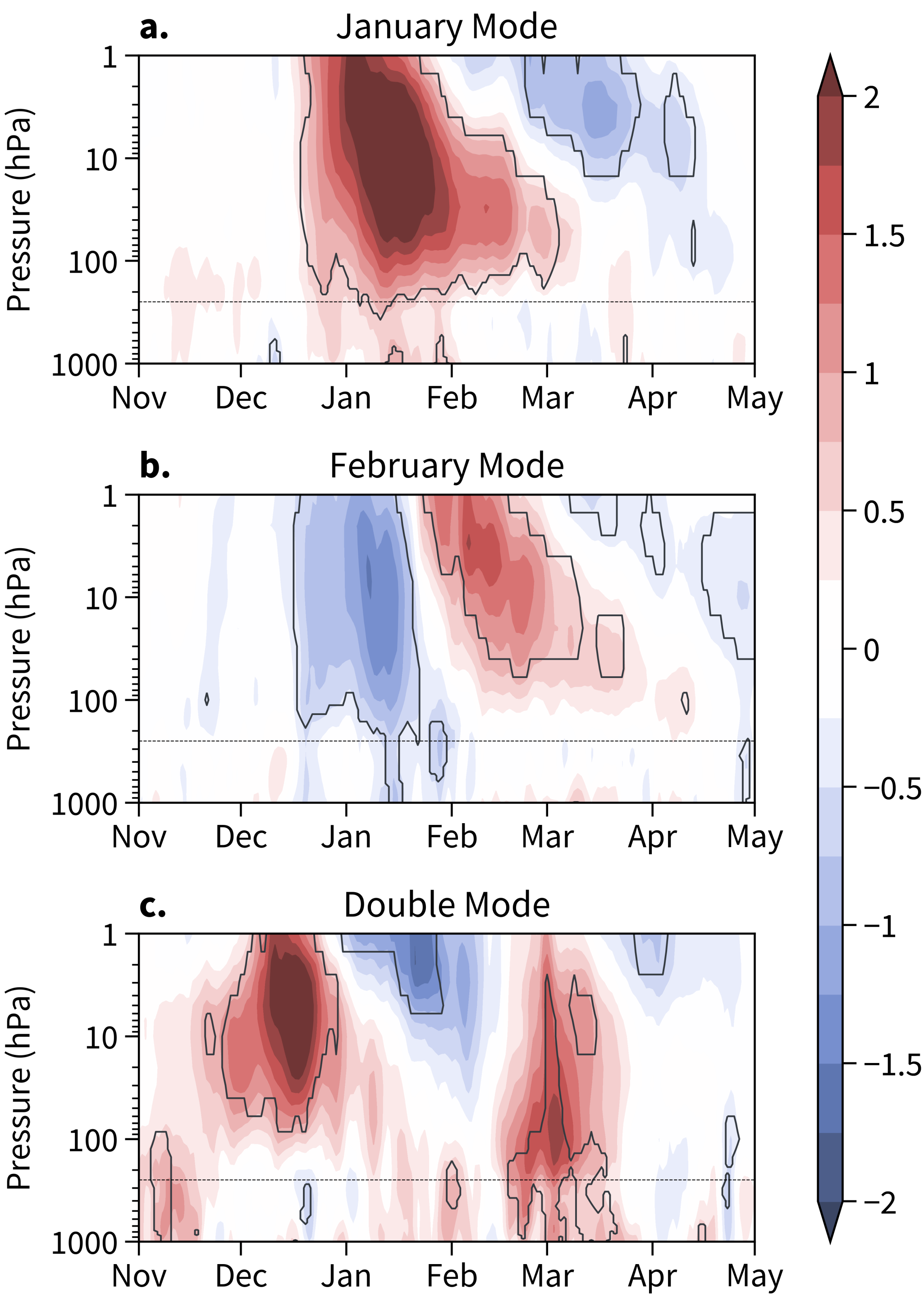

Figure 3. Mean time-height development of the northern annular mode indices for the winters associated with the three perturbed scenarios: the January Mode (a), the February Mode (b), and the Double Mode (c). The indices have daily resolution and are non-dimensional. Negative values (blue) corresponds to a strong polar vortex and positive values (red) to a weak polar vortex. The black lines contour areas with statistical significance at the 95% level according to a Student's t test. The horizontal black dashed lines indicate the approximate delimitation between the troposphere and the stratosphere.

4.3 Surface impacts at 1000 hPa

Figure 4 illustrates the evolution of monthly mean geopotential anomalies at 1000 hPa for the three perturbed scenarios from November to March. The stippled areas indicate the regions of highest significance according to the Student's t-test.

For the January mode, it can be observed that winters begin in November with a few surface signals of high significance: a positive anomaly over the Barent Sea and a negative anomaly in Western Europe. In December, significant signals are found across the investigated area. Therefore, winters typically exhibit a geopotential dipole with strong positive anomalies over Siberia and Asia, while significant negative anomalies cover the center and Northwest America. Interestingly, these surface signals display a wave-1-like pattern, coinciding with significant wave-1 activity diagnosed in the middle stratosphere before the occurrence of ISSWs for the January mode (see Fig. 8a in Mariaccia, Keckhut, and Hauchecorne (2022)). Thus, these results suggest that the surface pattern observed in December acts as a precursor to a specific wave-1 activity propagating upward from the troposphere and disturbing the stratospheric circulation, which in turn impacts the surface in the following months. This connection exemplifies the two-way troposphere-stratosphere coupling that takes place in the northern hemisphere during winter. In January, which is when the ISSW is expected to occur for winters associated with this mode, strong positive anomalies are observed at the pole and eastern Siberia, while negative anomalies are found in southern Europe and Northeast America. This pattern is typical of the negative phase of the AO. It is consistent with the NAM indices showing a downward propagation of positive anomalies in January (see Fig. 3). The positive anomaly persists at the pole until March but exhibits a rotational motion over the months. In February, this positive anomaly signal extends further over northern Canada, while in March, it covers Iceland and a part of the Pacific, with an overall decrease in significance.

Regarding the February mode, surprisingly, opposite signals are observed compared to the January mode, particularly for the months from November to January, confirming that these two modes possess very different initial surface conditions. In November, winters tend to have a negative anomaly over the Barent Sea, while a positive anomaly, though not highly significant, is observed in Western Europe. In December, the previous negative anomaly covers a portion of Siberia, and another negative anomaly appears over the west of Greenland, while a positive anomaly is observed over the U.S. West Coast. Another positive anomaly is found over Western Europe but lacks high significance. Interestingly, this surface pattern exhibits a wave-2-like pattern, especially for the negative signals, aligning with the period when wave-2 activity in the stratosphere increases for this mode (see Fig. 8b in Mariaccia, Keckhut, and Hauchecorne (2022)). Therefore, similar to the January mode, this surface pattern serves as an indicator of a future weak polar vortex generated by an ISSW in February. More generally, these results support the idea that December is a crucial month for identifying and anticipating the occurring scenario. In January, a negative anomaly is present at the pole, while a positive anomaly is observed in western Europe, albeit with low significance. Again, this result aligns with the NAM indices computed for this mode, which indicate a descent of negative anomalies during this period. This pattern corresponds to the positive phase of the AO. As expected, no significant signals are found in February when the ISSW is expected to occur, confirming that the anomaly does not reach the surface. Only a small positive anomaly signal in the Bering Sea tends to be recurrent in February, albeit with significance. In March, only a negative anomaly is present over the north of the U.K., while a positive anomaly is found over Northeast America. Therefore, these weak surface signals following the ISSW confirm that the overall troposphere evolves somewhat independently from the stratosphere.

Unlike the January and February modes, the Double mode exhibits strong signals in November, with a positive anomaly over the pole and the Barent Sea, while negative anomalies cover southern Europe and the Bering Sea. This pattern shares similarities with the one observed in December for the January mode, i.e., a wave-1-like pattern that can

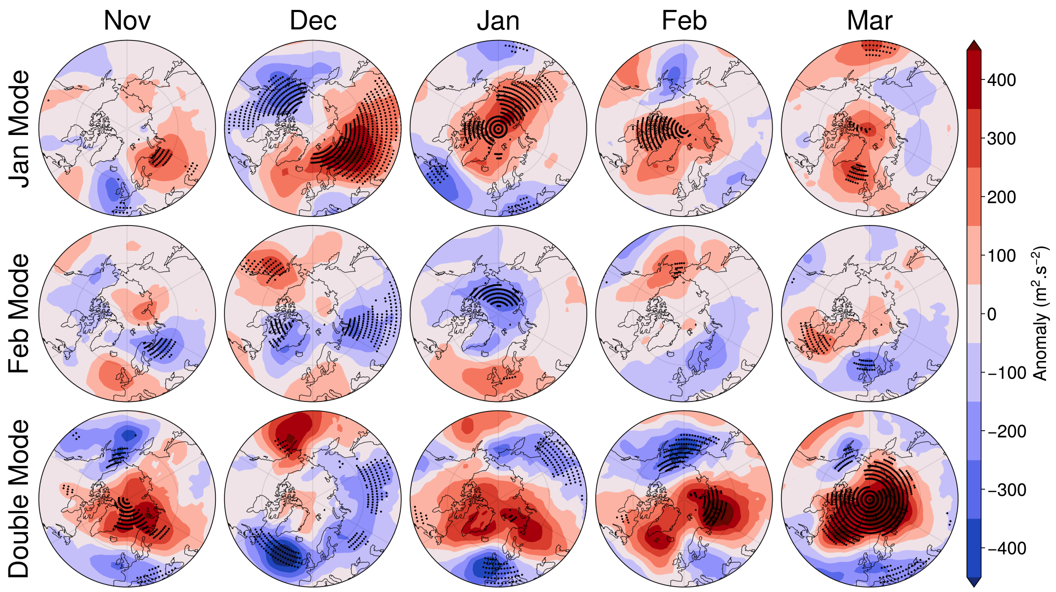

Figure 4. Monthly mean geopotential anomaly at 1000 hPa from 40°N poleward in the northern hemisphere for the three perturbed scenarios from November to March. Blue and red shaded regions respectively correspond to negative and positive geopotential anomalies. Stippled areas show statistical significance at the 95% level according to a Student's t test.

act as a precursor to the expected ISSW in the following month. In December, significant negative anomalies cover the North Atlantic Ocean and Eurasia, while a positive anomaly is present over the Bering Sea. Although the first ISSW occurs in December, there is no immediate downward propagation of the positive anomaly, as shown in Figure 3, where the descent into the troposphere occurs later in January and February. However, a significant positive anomaly is found in January, covering North America, the pole, and the land around the Barent Sea, albeit with low significance. Meanwhile, negative anomalies are present in Western Europe and China. In February, a significant positive anomaly over northern Siberia suggests that the stratospheric anomaly finally reached the surface. Simultaneously, a significant negative anomaly is present over the Bering Sea. Finally, in March, a negative phase of the AO is observed again due to the effect of the second ISSW, with a significant positive anomaly covering the entire pole, Greenland, and a northern part of Siberia.

Thus, based on Figure 4, it is evident that these three perturbed modes exhibit distinct surface signature evolutions throughout winters before and after the occurrences of ISSWs. However, there are similarities in the initial surface conditions and surface impacts between the January and Double modes, which are opposite to those observed for the February mode. Specifically, for the January and Double modes, a wave-1-like pattern is present at the surface in December and November, respectively, and the positive geopotential anomaly tends to propagate from the stratosphere to the surface after an ISSW, generally inducing a negative phase of the AO. In contrast, although the February mode displays a wave-2-like pattern at the surface in December, ISSWs occurring in February do not have subsequent impacts on the surface in the following months. Consequently, these perturbed scenarios exhibit precursors at the surface at the beginning of winter, particularly in December, which are likely responsible for the observed wave activity in the stratosphere and, therefore, appear crucial for anticipating the subsequent winter months. Regarding FSWs, their occurrence does not seem to significantly impact the surface, regardless of the perturbed mode. The investigation of the unperturbed mode and its two sub-modes, DFW and RFW, is presented in the next section.

5 Unperturbed Vortex Scenario

5.1 NAM evolutions

Figure 5 presents the NAM indices for the DFW and RFW modes, following a similar format to Figure 3. In line with expectations, both sub-modes exhibit a negative anomaly in the stratosphere, indicative of a persistent polar vortex that extends until the end of winter, finishing with either dynamical or radiative FSWs.

For the DFW mode, a negative anomaly forms on average in the stratosphere around 10 hPa starting in December. This negative anomaly propagates downward, gradually encompassing the entire stratosphere while intensifying until the end of February, reaching a peak around 30 hPa. The negative anomaly persists in the stratosphere until the end of February, at which point it initiates descent towards the troposphere, approaching the tropopause. Consequently, the negative anomalies reach the Earth's surface until the end of March. Interestingly, in early March, a positive anomaly appears at the top of the diagram. This positive anomaly corresponds to the occurrence of a dynamical FSW, which disrupts the polar vortex, resembling but with less intensity than the ISSWs observed in the three perturbed scenarios. Throughout March, this tilted positive anomaly propagates downward and reaches the lower stratosphere in April, but it does not significantly penetrate into the troposphere.

Regarding the RFW mode, weak but discernible anomaly signals are present in November, with a positive anomaly in the stratosphere and a negative anomaly in the troposphere. This positive anomaly descends while gaining strength, reaching the tropopause region and influencing the troposphere in December. Concurrently, a robust negative anomaly begins to form in the upper stratosphere. This negative anomaly propagates downward, covering the entire stratosphere from mid-January to mid-April while maintaining its intensity, indicating a persistently strong polar vortex throughout winter. From January to April, the tropospheric surface experiences the effects of this robust polar vortex, as anomalies persist just above the tropopause, facilitating their spread into the troposphere. It is important to note that this scenario represents the average evolution of only five winters, making this result statistically less robust than others. Notably, the surface is strongly influenced by the final stages of the wintertime stratospheric circulation in April, coinciding with the occurrence of the radiative FSW.

In the next section, we delve into the surface impact analysis for both sub-modes, examining the affected regions over the course of several months.

5.2 Surface impacts at 1000 hPa

Figure 6 illustrates the monthly mean geopotential anomaly at 1000 hPa from January to April for both the DFW and RFW modes. The decision to display only the months when stratospheric anomalies strongly impact the surface was made because undisturbed winters do not exhibit significant signals before January (not shown).

Regarding the DFW mode, significant anomalies are observed at the surface in February and March. In both months, a substantial negative anomaly is present at the pole and north of America, while a positive anomaly is observed in central Europe and northern Europe in February and March, respectively. Additionally, a notable negative anomaly tends to appear in the Pacific Ocean in March. Thus, these two months share a similar pattern, characteristic of a positive phase of the AO. The positive AO phase in the DFW mode is induced by a downward propagation of stratospheric anomalies, confirming their connection with strong polar vortex events. Furthermore, the surface signal in the DFW mode exhibits a wave-1-like pattern, consistent with the wave activity diagnosed in the stratosphere during this period (Mariaccia, Keckhut, & Hauchecorne, 2022), indicating a vertical connection from the surface to the upper stratosphere. This persistent wave-1 activity is likely the

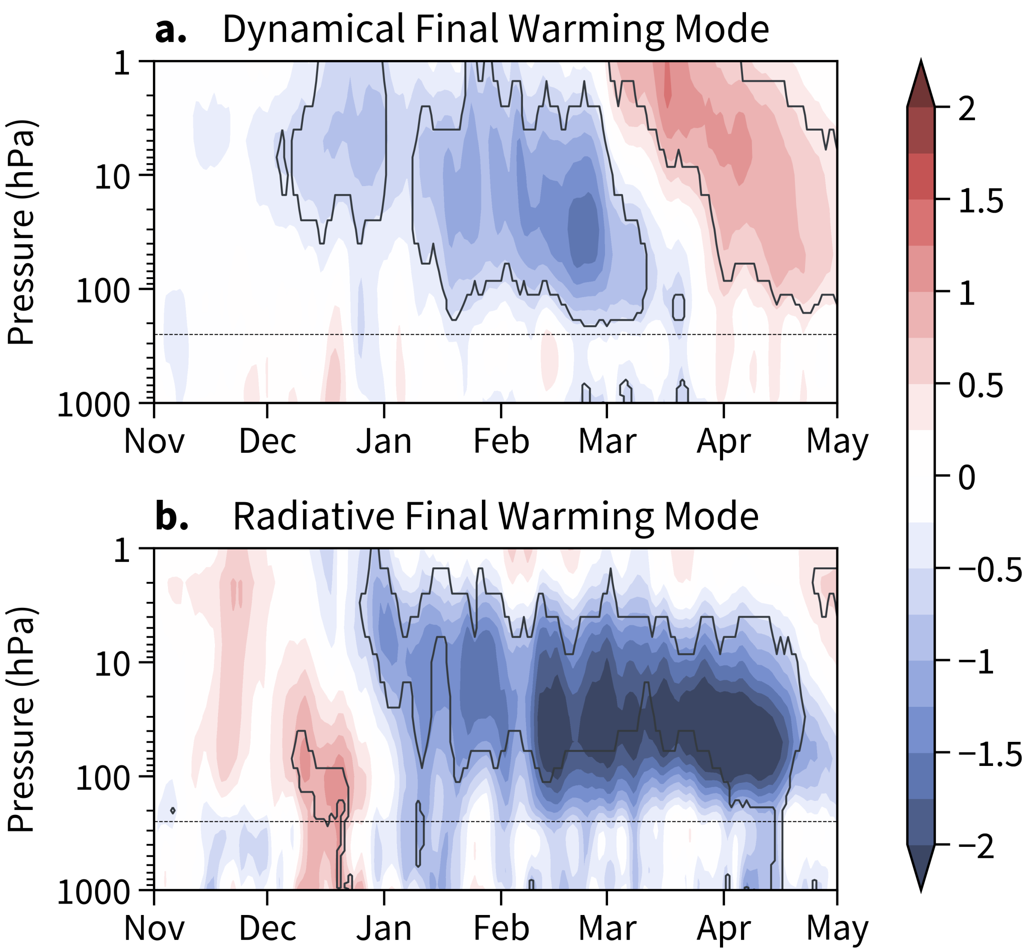

Figure 5. Mean time-height development of the northern annular mode indices for the winters associated with the two sub-modes composing the unperturbed scenario: the Dynamical Final Warming Mode (a) and the Radiative Final Warming Mode (b). The indices have daily resolution and are non-dimensional. Negative values (blue) corresponds to a strong polar vortex and positive values (red) to a weak polar vortex. The black lines contour areas with statistical significance at the 95% level according to a Student's t test. The horizontal black dashed lines indicate the approximate delimitation between the troposphere and the stratosphere.

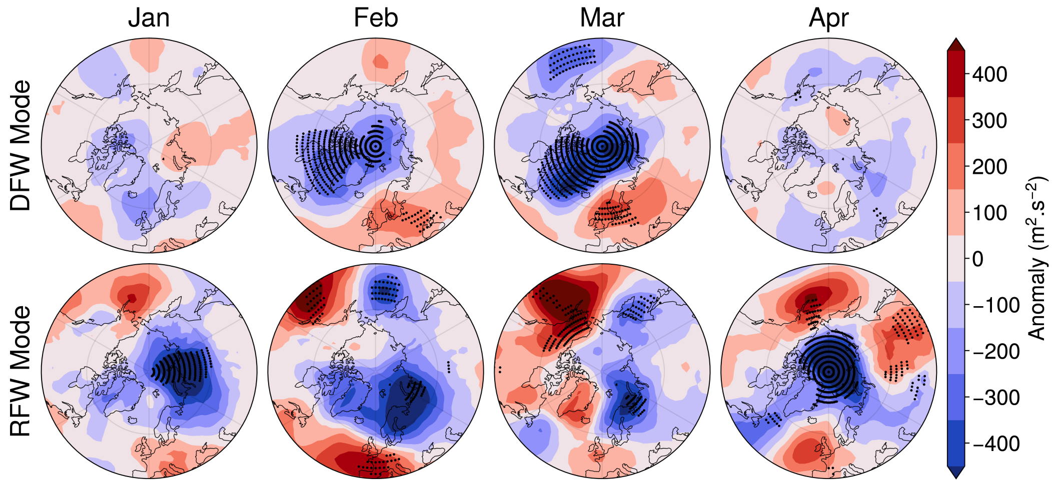

Figure 6. Monthly mean geopotential anomaly at 1000 hPa from 40°N poleward in the northern hemisphere for the two sub-modes composing the unperturbed scenario from November to March. Blue and red shaded regions respectively correspond to negative and positive geopotential anomalies. Stippled areas show statistical significance at the 95% level according to a Student's t test.

cause of the dynamical FSW occurring in April, similar to the disturbed scenarios. However, unlike wave-1-driven ISSWs, the final pattern in April is not influenced by the positive stratospheric anomaly generated by the dynamical FSW, as seen in the NAM evolution (see Fig. 5).

In contrast, the RFW mode shows significant signals throughout the studied period. In January, a highly significant negative anomaly is found from the pole to the north of Siberia, in agreement with the descending stratospheric anomaly during this period (see Fig. 5a). In February, the negative anomaly persists but with reduced significance, and an additional negative anomaly appears in the Pacific below the Bering Sea. Positive anomalies are observed in the Pacific near the U.S. west coast and in western Europe. In March, the preceding negative anomalies shift slightly to northern Europe and Russia's east coast, respectively, while the previous positive anomaly over western Europe diminishes, and the one in the Pacific moves westward and spreads over Alaska. The RFW mode's NAM evolution suggests that the surface patterns in February and March are less affected by the stratosphere due to the less significant descent of anomalies during these months.

Moreover, the surface signal in March exhibits a wave-2-like pattern that aligns with the peak of wave-2 activity found in the stratosphere during this period (Mariaccia, Keckhut, & Hauchecorne, 2022). This result confirms the vertical connection through wave activity when the polar vortex is strong, characterized by westerly winds that enable planetary wave propagation. However, despite significant wave-2 activity in March, there is no generation of stratospheric anomalies associated with triggering an ISSW, indicating the essential role of wave-1, which exhibits low activity during this period. In April, a strong and significant negative anomaly is found at the pole, while positive anomalies are observed over the Bering Sea and the center of Siberia and China. This pattern reflects a positive phase of the Arctic Oscillation, similar to what is found in February and March of the DFW mode. It aligns with the last observed anomaly descent in the NAM evolution. Beyond April, no further stratospheric anomalies are present due to the return of solar radiation, dissipating the polar vortex.

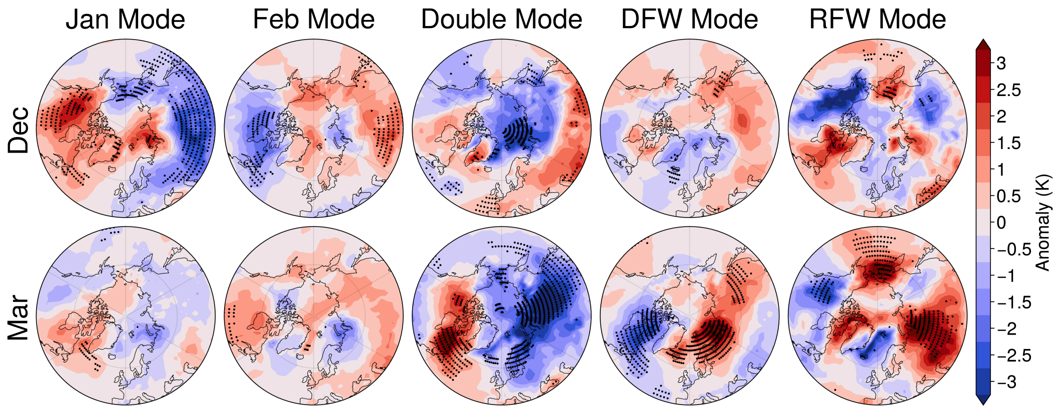

Figure 7. Monthly mean temperature anomaly at 1000 hPa from 40°N poleward in the northern hemisphere for each scenario in December and March. Stippled areas show statistical significance at the 95% level according to a Student's t test.

In summary, winters associated with the two sub-modes of the unperturbed scenario exhibit similar surface patterns significantly impacted by the downward propagation of negative stratospheric anomalies during the winter months. A positive Atlantic Oscillation emerges at the surface when the FSW occurs in both the DFW and RFW modes. These surface patterns differ notably from those obtained in the three perturbed scenarios, which are characterized by negative AO patterns after ISSWs. Therefore, the positive AO patterns observed in March and April for the DFW and RFW modes signify the disappearance of the polar vortex. This finding confirms that the timing and nature of FSWs are crucial for understanding the temporal shift in observed ground impacts. However, no significant surface harbingers are found in December and preceding months, suggesting that the FSW type is influenced more by January onwards rather than early winter.

6 Impacts on Surface Temperature

To investigate the effects of different scenarios on climate during winter, which is crucial for seasonal-scale weather forecasts, we present the monthly mean temperature anomaly at 1000 hPa in December and March in the northern hemisphere for each scenario (Fig. 7). Additionally, since the Double mode exhibits significant geopotential signals earlier in winter (Fig. 4), we also include the mean temperature anomaly at 1000 hPa in November for the Double mode in Figure 8. Generally, positive geopotential anomalies are associated with negative temperature anomalies, and negative geopotential anomalies are associated with positive temperature anomalies during the same period.

In December, it is not surprising to find that the January and February modes exhibit opposite dipole signals, consistent with the mean geopotential anomaly shown previously for this month. The January mode shows negative temperature anomalies ranging from -1 to -3 K over Eurasia, while positive anomalies of +1 to +2.5 K are observed over North America and Greenland. Notably, this temperature anomaly pattern over Eurasia in December bears similarities, but with higher significance, to the surface temperature anomalies found in the -30 to 0 days before Displacement Sudden Stratospheric Warming (SSW) events (Mitchell et al., 2013). In contrast, the February mode demonstrates less significant signals, with temperature anomalies only reaching +1.5 K in Siberia and -1.5 K in North America.

Interestingly, the mean temperature anomaly patterns observed in December and January (not shown here) for the February mode do not correspond to the precursor stage for either Displaced or Splitting events suggesting a mixed signal. Regarding the geopotential

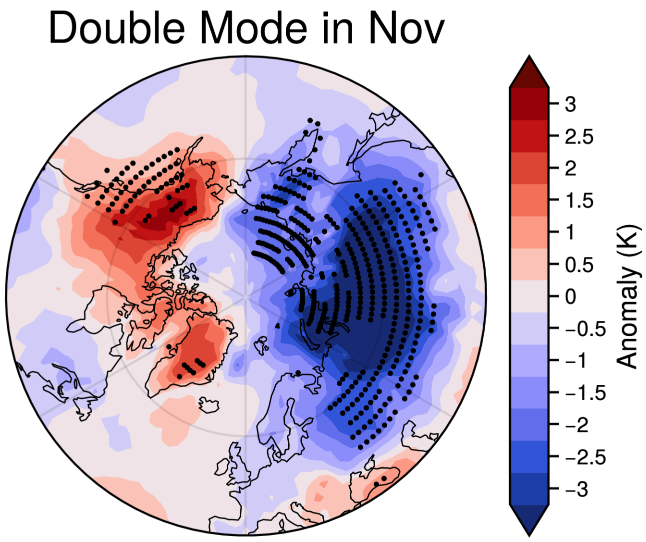

Figure 8. Monthly mean temperature anomaly at 1000 hPa from 40°N poleward in the northern hemisphere for the Double mode in November. Stippled areas show statistical significance at the 95% level according to a Student's t test.

anomaly, the temperature anomaly observed in November for the Double mode is similar to the one observed in December for the January mode, but with stronger negative anomalies over a large part of Eurasia exceeding -3 K, and positive anomalies of +1.5 K mainly covering North West America and Greenland. Despite the weak significance in December, the Double mode exhibits positive and negative temperature anomalies in the south and north of Siberia, respectively, indicating a warming of the Eurasia region when the first SSW of this scenario occurs in the stratosphere. These surface temperature patterns, similar to the geopotential patterns, can be considered precursors of these perturbed scenarios, providing further evidence that troposphere-stratosphere coupling substantially influences the winter climate in the northern hemisphere. These findings are of great interest for improving sub-to-seasonal forecasts. However, for the December month, the signals observed for the DFW and RFW modes have weak significance, consistent with the NAM evolution during this period. Therefore, the absence of surface signals with high significance up to December indicates that the winter is following an unperturbed scenario.

In March, the January and February modes exhibit similarities but do not show mean temperature anomalies with high significance, suggesting that the surface climate at this period is no longer influenced by stratospheric anomalies, which aligns with the observed NAM evolutions (Fig. 3a-b). Hence, surface precursors can anticipate these two scenarios in December, but they are not indicative of a specific surface climate at the end of winter. It is noteworthy that their surface patterns in March are similar to those observed for Splitting and Displacement events in their decay phase (Mitchell et al., 2013), making it challenging to draw meaningful comparisons or deductions.

Interestingly, the Double mode shows nearly identical surface signals in March as those observed in November, but with positive temperature anomalies covering a larger area in North East America exceeding +3 K. Thus, the surface harbinger found in November associated with the Double mode is similar to the effect generated by the second SSW occurring at the end of February. Consequently, the Double mode is a unique mode with a strong impact on the northern hemisphere's surface climate from November to March.

Finally, in March, the surface signals observed for the DFW and RFW modes are opposite to those found for the Double mode but similar to those observed in December for the February mode. The DFW mode shows a significant positive temperature anomaly exceeding +3 K over the Barent Sea region, ranging between 1 and 2 K in East Siberia, and negative anomalies averaging -1.5 K over North-East America. Similarly, the RFW mode exhibits positive anomalies exceeding +2.5 K on average over the center of Siberia and the Bering Sea region, while substantial negative temperature anomalies of -3 K and below are found over West America, Iceland, and Svalbard. Consequently, the similar temperature surface patterns between the DFW and RFW modes indicate that the type of final stratospheric warming does not determine a specific meteorological impact.

In general, these different surface harbingers and responses provide evidence for the existence of a connection between early and late winter due to stratosphere-troposphere coupling, confirming its significant influence on the climate in the northern hemisphere during wintertime.

7 Summary

In this study, we have conducted an investigation into the coupling between the stratosphere and troposphere for both perturbed and unperturbed scenarios, as established in a previous work by Mariaccia, Keckhut, and Hauchecorne (2022). By analyzing the time-height evolutions of the mass-weighted divergence anomaly of the Eliassen-Palm flux, averaged in the latitude range of 50-70°N, we have found that the mean eddy heat and momentum flux primarily influence the upper stratosphere. These findings are consistent with the zonal mean temperature and zonal mean zonal wind evolutions at 10 hPa within the same latitude range. In addtion, the divergence evolutions at 1000 hPa reveal that the dynamics in the upper stratosphere is potentially influenced by the surface some weeks in advance. Moreover, our analysis of the contributions from wave-1 and wave-2 to this divergence anomaly aligns with the wave activities associated with each scenario as reported earlier. Notably, we have observed that wave-2 plays a role in reinforcing the polar vortex following the occurrence of the ISSW for the January and Double modes.

Regarding the unperturbed scenario, we have identified frequent oscillations in the sign of the divergence in the upper stratosphere. These oscillations provide a physical explanation as to why the polar vortex remains strong during this scenario. These wave activity diagnoses enhance our understanding of the distinct dynamical behaviors exhibited by these scenarios and their impact on polar vortexes. Such inferences are crucial for potential simulations of these scenarios using mechanistic models.

We have also found that the time-height Northern Annular Mode (NAM) evolutions associated with each scenario align temporally with the phases of reinforcement and weakening of the polar vortex caused by ISSWs and FSWs. The discrepancies observed in these NAM evolutions, particularly in the descent of stratospheric anomalies caused by ISSWs or strong polar vortex events, provide confirmation that these scenarios affect the stratosphere and troposphere differently throughout the winter. Consequently, these novel findings offer compelling evidence of stratosphere-troposphere coupling during the winter months. Moreover, consistent with most studies, our results suggest that downward propagation toward the tropopause is crucial for enabling the descent of stratospheric anomalies to the surface, irrespective of their sign. In a broader sense, these outcomes verify that these scenarios not only represent a wind and temperature evolution at the edge of the polar vortex but also distinct states of the stratosphere and troposphere that influence each other during the winter months in the northern hemisphere. Overall, the diverse NAM evolutions demonstrate unique vertical and temporal connections in wintertime, which are of significant interest for climate forecasts.

When comparing our results with the classification based on vortex geometry, specifically displaced or splitting events, as performed by Mitchell et al. (2013), we have encountered inconsistencies between the NAM evolutions, surface temperature anomalies, and observed wave activity for perturbed scenarios. These discrepancies are likely attributed to the different approaches in the classifications, one based on the dates of SSW events and the other on main winter typologies, thereby hindering meaningful comparisons. Additionally, uncertainties exist in the method used to identify the polar vortex geometry. Consequently, establishing a direct relationship between a specific polar vortex geometry and each scenario based on this comparison is not evident. Thus, the timing of ISSWs appears to be more crucial than vortex geometry in attempting to predict a descent of stratospheric anomalies.

After examining the surface patterns of geopotential and temperature anomalies, several important findings emerge regarding the precursors and tropospheric responses during winter for each scenario:

1. January mode:
   - In December, there is a dipole structure of mean geopotential anomalies, with positive anomalies over Eurasia and negative anomalies over North-West America. This pattern is accompanied by mean temperature anomalies of -2 K over Eurasia and +2 K over North America. These surface patterns act as a precursor to the occurrence of an ISSW in January.
   - In January and February, a negative phase of the AO is observed at the surface due to the descent of positive stratospheric anomalies generated by the ISSW.
2. February mode:
   - In December, an opposite signal to the January mode is observed, with negative geopotential anomalies over Siberia and West Greenland, and positive anomalies over the U.S. West Coast. This surface signal exhibits a wave-2-like pattern, acting as a harbinger of the ISSW in February. Associated temperature anomalies reach, on average, +1.5 K over Siberia and -1.5 K over North America.
   - In January, a positive phase of AO appears at the surface due to the descent of negative stratospheric anomalies, indicating the presence of a strong polar vortex. From February onwards, no significant signals indicate that the stratosphere no longer influences the surface.
3. Double mode:
   - In November, the mean geopotential anomaly shows positive anomalies over the pole and the Barent Sea, and negative anomalies over southern western Europe and the Bering Sea. This signal shares similarities with the December pattern observed for the January mode. Associated with these anomalies are surface temperature anomalies exceeding -3 K over Eurasia and around +1.5 K over North West America and Greenland. These patterns exhibit a wave-1-like structure, acting as a precursor for the Double mode.
   - In January and February, the first ISSW causes the descent of the stratospheric anomaly into the troposphere. This leads to positive geopotential anomalies over Greenland and the Barent Sea, and negative anomalies over western Europe and China in January, and the Bering Sea in February.
   - In March, the second ISSW generates a significant descent of the stratospheric anomaly, resulting in a substantial negative AO phase. This is associated with temperature anomalies exceeding +3 K over North East America and -3 K over Eurasia.
4. DFW mode:
   - Consistent with its NAM evolution, no surface precursor exists for this mode, and no significant anomalies appear before February.

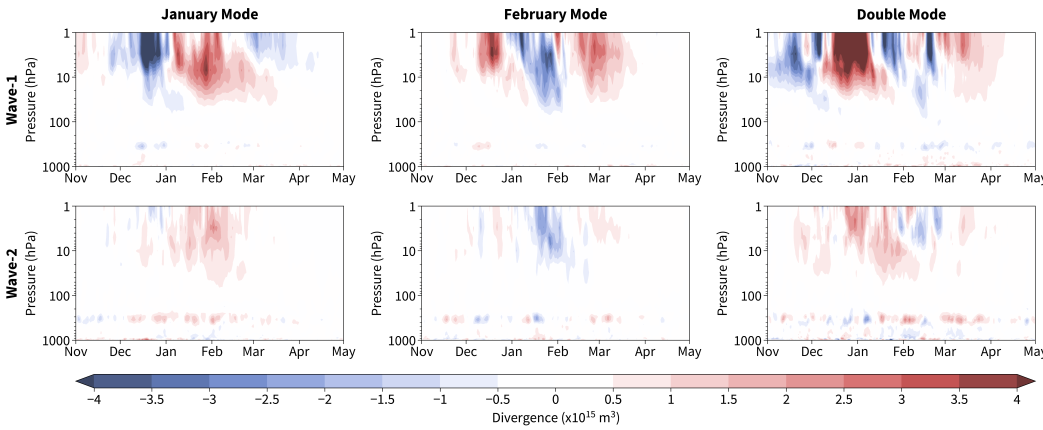

Figure A1. Contributions from Wave-1 and Wave-2 in the mean time-height development of the anomaly of the mass weighted divergence of Eliassen-Palm flux in the latitude range 50-70°N for the three perturbed scenarios. Shaded negative (blue) and positive (red) values correspond to a deceleration and acceleration of the zonal wind, respectively.

- In February and March, a positive AO phase is observed, accompanied by a positive geopotential anomaly concentrated in Western Europe. In March, this surface pattern is associated with temperature anomalies exceeding +3 K over the Barent Sea region, and on average, +1.5 K over East Siberia. Negative anomalies of -1.5 K, on average, are found over North-East America.

5. RFW mode:
   - Negative stratospheric anomaly descents occur from January to April during this mode. In January, a positive AO-like phase pattern is observed.
   - From February to March, a wave-2-like pattern emerges with positive geopotential anomalies over the U.S. West coast and western Europe, and negative anomalies over the Barent Sea region and Siberia's East coast.
   - Finally, in April, a pronounced positive phase of the AO emerges when the polar vortex disappears.

These findings significantly contribute to our understanding of stratosphere-troposphere coupling during the winter in the northern hemisphere, with important implications for sub-seasonal to seasonal climate forecasts. Future research should employ mechanistic models to test whether these precursors and specific wave activities associated with each scenario can simulate ISSWs with the expected timing. Furthermore, investigating the causes of stratospheric anomaly entry into the troposphere would be beneficial. Additional investigations are necessary to better comprehend the triggers for each scenario, with one potential avenue being to explore links with sea ice concentrations and thicknesses at the beginning of winter.

Appendix A Contributions from Wave-1 and Wave-2 in the divergence of Eliassen-Palm flux

Acknowledgments

This work was performed within the framework of the European ARISE project and was funded by the French Educational Ministry with EUR IPSL. Copernicus Climate Change Service (C3S): ERA5: Fifth generation of ECMWF atmospheric reanalyses of the global

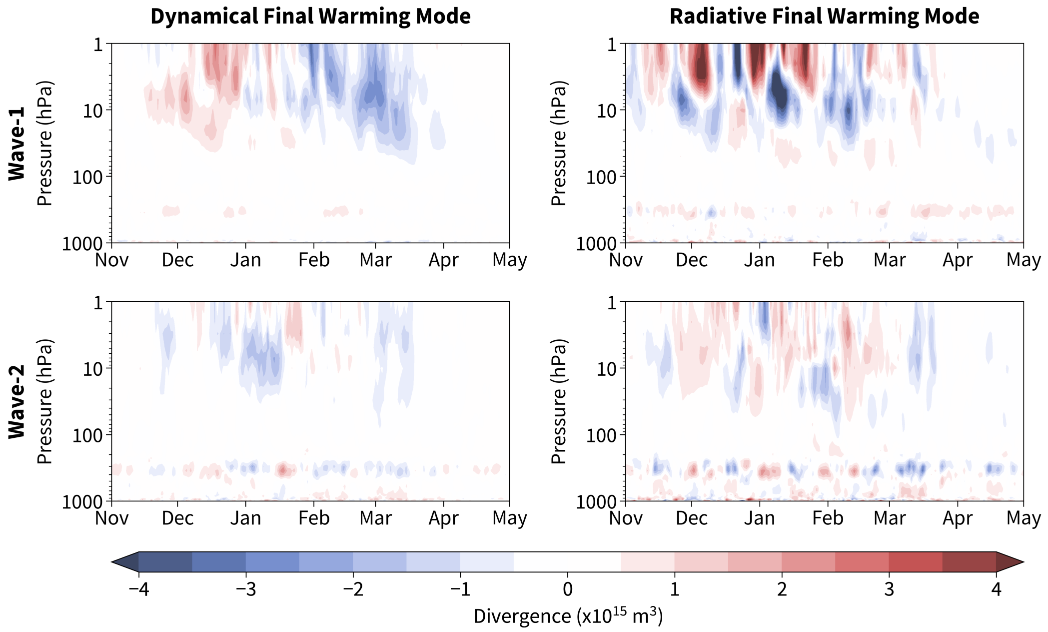

Figure A2. Contributions from Wave-1 and Wave-2 in the mean time-height development of the anomaly of the mass weighted divergence of Eliassen-Palm flux in the latitude range 50-70°N for the two sub-modes composing the unperturbed scenario. Shaded negative (blue) and positive (red) values correspond to a deceleration and acceleration of the zonal wind, respectively.

climate. Copernicus Climate Change Service Climate Data Store (CDS), accessible at: `https://cds.climate.copernicus.eu/cdsapp#!/home`.

References

Afargan-Gerstman, H., & Domeisen, D. I. V. (2020). Pacific modulation of the north atlantic storm track response to sudden stratospheric warming events. *Geophysical Research Letters*, *47*(2), e2019GL085007. doi: https://doi.org/10.1029/2019GL085007

Andrews, D. G., Mahlman, J. D., & Sinclair, R. W. (1983). Eliassen-palm diagnostics of wave-mean flow interaction in the gfdl "skyhi" general circulation model. *Journal of Atmospheric Sciences*, *40*(12), 2768 - 2784. doi: https://doi.org/10.1175/1520-0469(1983)040⟨2768:ETWATM⟩2.0.CO;2

Ayarzagüena, B., Langematz, U., & Serrano, E. (2011). Tropospheric forcing of the stratosphere: A comparative study of the two different major stratospheric warmings in 2009 and 2010. *Journal of Geophysical Research: Atmospheres*, *116*(D18). doi: https://doi.org/10.1029/2010JD015023

Baldwin, M. P., & Dunkerton, T. J. (2001). Stratospheric harbingers of anomalous weather regimes. *Science*, *294*(5542), 581-584. doi: 10.1126/science.1063315

Baldwin, M. P., & Thompson, D. W. (2009). A critical comparison of stratosphere–troposphere coupling indices. *Quarterly Journal of the Royal Meteorological Society*, *135*(644), 1661-1672. doi: https://doi.org/10.1002/qj.479

Bancalá, S., Krüger, K., & Giorgetta, M. (2012). The preconditioning of major sudden stratospheric warmings. *Journal of Geophysical Research: Atmospheres*, *117*(D4). doi: https://doi.org/10.1029/2011JD016769

Barriopedro, D., & Calvo, N. (2014). On the relationship between enso, stratospheric sudden warmings, and blocking. *Journal of Climate*, *27*(12), 4704 - 4720. doi: https://doi.org/

10.1175/JCLI-D-13-00770.1

Butler, A. H., & Domeisen, D. I. V. (2021). The wave geometry of final stratospheric warming events. *Weather and Climate Dynamics*, *2*(2), 453–474. doi: 10.5194/wcd-2-453-2021

Butler, A. H., Seidel, D. J., Hardiman, S. C., Butchart, N., Birner, T., & Match, A. (2015). Defining sudden stratospheric warmings. *Bulletin of the American Meteorological Society*, *96*(11), 1913 - 1928. doi: https://doi.org/10.1175/BAMS-D-13-00173.1

Charlton, A. J., & Polvani, L. M. (2007). A new look at stratospheric sudden warmings. part i: Climatology and modeling benchmarks. *Journal of Climate*, *20*(3), 449 - 469. doi: https://doi.org/10.1175/JCLI3996.1

Cohen, J., & Jones, J. (2011). Tropospheric precursors and stratospheric warmings. *Journal of Climate*, *24*(24), 6562 - 6572. doi: https://doi.org/10.1175/2011JCLI4160.1

Domeisen, D. I. (2019). Estimating the frequency of sudden stratospheric warming events from surface observations of the north atlantic oscillation. *Journal of Geophysical Research: Atmospheres*, *124*(6), 3180-3194. doi: https://doi.org/10.1029/2018JD030077

Edmon, H. J., Hoskins, B. J., & McIntyre, M. E. (1980). Eliassen-palm cross sections for the troposphere. *Journal of Atmospheric Sciences*, *37*(12), 2600 - 2616. doi: https://doi.org/10.1175/1520-0469(1980)037⟨2600:EPCSFT⟩2.0.CO;2

Esler, J. G., & Scott, R. K. (2005). Excitation of transient rossby waves on the stratospheric polar vortex and the barotropic sudden warming. *Journal of the Atmospheric Sciences*, *62*(10), 3661 - 3682. doi: https://doi.org/10.1175/JAS3557.1

Hauchecorne, A., Claud, C., Keckhut, P., & Mariaccia, A. (2022). Stratospheric final warmings fall into two categories with different evolution over the course of the year. *Communications Earth & Environment*, *3*(1), 4. doi: https://doi.org/10.1038/s43247-021-00335-z

Hersbach, H., Bell, B., Berrisford, P., Hirahara, S., Horányi, A., Muñoz-Sabater, J., ... Thépaut, J.-N. (2020). The era5 global reanalysis. *Quarterly Journal of the Royal Meteorological Society*, *146*(730), 1999-2049. doi: https://doi.org/10.1002/qj.3803

Jucker, M. (2021). Scaling of eliassen-palm flux vectors. *Atmospheric Science Letters*, *22*(4), e1020. doi: https://doi.org/10.1002/asl.1020

Karpechko, A. Y., Hitchcock, P., Peters, D. H. W., & Schneidereit, A. (2017). Predictability of downward propagation of major sudden stratospheric warmings. *Quarterly Journal of the Royal Meteorological Society*, *143*(704), 1459-1470. doi: https://doi.org/10.1002/qj.3017

Kidston, J., Scaife, A. A., Hardiman, S. C., Mitchell, D. M., Butchart, N., Baldwin, M. P., & Gray, L. J. (2015). Stratospheric influence on tropospheric jet streams, storm tracks and surface weather. *Nature Geoscience*, *8*(6), 433–440. doi: https://doi.org/10.1038/ngeo2424

Kodera, K., Funatsu, B. M., Claud, C., & Eguchi, N. (2015). The role of convective overshooting clouds in tropical stratosphere–troposphere dynamical coupling. *Atmospheric Chemistry and Physics*, *15*(12), 6767–6774. doi: 10.5194/acp-15-6767-2015

Kodera, K., Mukougawa, H., Maury, P., Ueda, M., & Claud, C. (2016). Absorbing and reflecting sudden stratospheric warming events and their relationship with tropospheric circulation. *Journal of Geophysical Research: Atmospheres*, *121*(1), 80-94. doi: https://doi.org/10.1002/2015JD023359

Mariaccia, A., Keckhut, P., & Hauchecorne, A. (2022). Classification of stratosphere winter evolutions into four different scenarios in the northern hemisphere. *Journal of Geophysical Research: Atmospheres*, *127*(13), e2022JD036662. doi: https://doi.org/10.1029/2022JD036662

Mariaccia, A., Keckhut, P., Hauchecorne, A., Claud, C., Le Pichon, A., Meftah, M., & Khaykin, S. (2022). Assessment of era-5 temperature variability in the middle atmosphere using rayleigh lidar measurements between 2005 and 2020. *Atmosphere*, *13*(2). doi: 10.3390/atmos13020242

Marlton, G., Charlton-Perez, A., Harrison, G., Polichtchouk, I., Hauchecorne, A., Keckhut, P., … Steinbrecht, W. (2021). Using a network of temperature lidars to identify temperature biases in the upper stratosphere in ecmwf reanalyses. *Atmospheric Chemistry and Physics*, *21*(8), 6079–6092. doi: 10.5194/acp-21-6079-2021

Matsuno, T. (1970). Vertical propagation of stationary planetary waves in the winter northern hemisphere. *Journal of Atmospheric Sciences*, *27*(6), 871 - 883. doi: https://doi.org/10.1175/1520-0469(1970)027⟨0871:VPOSPW⟩2.0.CO;2

Mitchell, D. M., Gray, L. J., Anstey, J., Baldwin, M. P., & Charlton-Perez, A. J. (2013). The influence of stratospheric vortex displacements and splits on surface climate. *Journal of Climate*, *26*(8), 2668 - 2682. doi: https://doi.org/10.1175/JCLI-D-12-00030.1

Nakagawa, K. I., & Yamazaki, K. (2006). What kind of stratospheric sudden warming propagates to the troposphere? *Geophysical Research Letters*, *33*(4). doi: https://doi.org/10.1029/2005GL024784

Runde, T., Dameris, M., Garny, H., & Kinnison, D. E. (2016). Classification of stratospheric extreme events according to their downward propagation to the troposphere. *Geophysical Research Letters*, *43*(12), 6665-6672. doi: https://doi.org/10.1002/2016GL069569

Thompson, D. W. J., & Wallace, J. M. (2001). Regional climate impacts of the northern hemisphere annular mode. *Science*, *293*(5527), 85-89. doi: 10.1126/science.1058958

Tripathi, O. P., Baldwin, M., Charlton-Perez, A., Charron, M., Eckermann, S. D., Gerber, E., … Son, S.-W. (2015). The predictability of the extratropical stratosphere on monthly time-scales and its impact on the skill of tropospheric forecasts. *Quarterly Journal of the Royal Meteorological Society*, *141*(689), 987-1003. doi: https://doi.org/10.1002/qj.2432

Vargin, P., Luk'yanov, A., & Kiryushov, B. (2020). Dynamic processes in the arctic stratosphere in the winter of 2018/2019. *Russian Meteorology and Hydrology*, *45*, 387–397. doi: https://doi.org/10.3103/S1068373920060011

Waugh, D. W., & Rong, P.-P. (2002). Interannual variability in the decay of lower stratospheric arctic vortices. *Journal of the Meteorological Society of Japan. Ser. II*, *80*(4B), 997–1012. doi: https://doi.org/10.2151/jmsj.80.997

Classification of Stratosphere Winter Evolutions Into Four Different Scenarios in the Northern Hemisphere: Part B Coupling With The Surface

A. Mariaccia[1], P. Keckhut[1], and A. Hauchecorne[1]

[1]Laboratoire Atmosphères, Milieux, Observations Spatiales, UMR 8190, Institut Pierre-Simon Laplace, Université Versailles-Saint Quentin, Université Paris-Saclay, 78280 Guyancourt, France.

Key Points:

- Distinct wave activity effects are diagnosed for each scenario.
- Each scenario possesses unique stratosphere-troposphere interaction in winter.
- Surface precursors in perturbed scenarios emerge in early winter, especially December.

Corresponding author: Alexis Mariaccia, `alexis.mariaccia@latmos.ipsl.fr`

Abstract

We have conducted an investigation into the coupling between the stratosphere and troposphere, focusing on perturbed and unperturbed scenarios of the northern hemisphere polar vortex. These scenarios were established in a previous study, which categorized the main winter typologies based on the timing of sudden stratospheric warmings (SSWs) and final stratospheric warmings (FSWs). Here, we further analyze the mass-weighted divergence of the Eliassen-Palm (EP) flux to confirm the association between these scenarios and the specific timing of momentum and heat flux deposition by planetary waves. Our analysis reveals that wave-1 and wave-2 contributions to this divergence confirm distinct wave activity effects in relation to these scenarios. Additionally, examining the evolutions of the Northern Annular Mode (NAM) provides further insight, demonstrating that these scenarios represent unique states of both the stratosphere and troposphere, which mutually influence each other during the winter months. Of particular interest is the observation of descending stratospheric anomalies into the troposphere following SSWs, often accompanied by a negative phase of the Arctic Oscillation (AO). Notably, we have made an important discovery regarding surface precursors for perturbed scenarios in early winter, specifically December. These surface precursors display wave-like patterns that align with the diagnosed wave activity in the upper stratosphere. This finding establishes a connection between early and late winter, highlighting the importance of these precursors. Consequently, our results enhance our ability to anticipate the behavior of the polar vortex and its impacts, thus holding significant implications for sub-seasonal to seasonal forecasts in the northern hemisphere.

Plain Language Summary

The stratosphere-troposphere coupling is a dynamic and important area of research, as it is widely recognized that the interactions between the stratosphere and troposphere significantly impact each other, particularly during the winter season. It has been established that accurately representing this coupling in climate models can lead to improvements in weather forecasting. One prominent phenomenon that exemplifies this coupling is sudden stratospheric warming (SSW), which occurs due to interactions between planetary waves and the mean flow in the stratosphere. SSW events can have notable effects on the surface, including potential shifts in extra-tropical storm tracks and the occurrence of severe cold-air outbreaks. Given the significant impacts of SSWs, the scientific community has been actively working towards classifying these events based on their characteristics and impacts. In a previous study, a novel classification scheme was introduced, which identified four distinct scenarios for the northern hemisphere polar vortex based on the timings of SSWs and final stratospheric warmings (FSWs). In this paper, we aim to evaluate the stratosphere-troposphere coupling for each of these scenarios during the winter months, with the goal of identifying potential associated precursors.

1 Introduction

The understanding of stratosphere-troposphere coupling is a crucial aspect of improving seasonal weather predictions in atmospheric sciences. This field of research has gained significant attention due to its impact on the mutual influence between the stratospheric polar vortex and the tropospheric circulation during the northern hemisphere winter. One of the key models, developed by Matsuno (1970), explains that variations in the strength of the wintertime stratospheric circulation are a result of the interaction between the mean flow and upward propagating planetary waves that transport westward momentum from the troposphere. These interactions can give rise to sudden stratospheric warming (SSW) events, characterized by increased polar cap temperatures, weakened polar vortex, and even the reversal of westerly winds in extreme cases. The subsequent stratospheric circulation anomalies can descend into the troposphere, influencing surface weather patterns for up to two months. Additionally, equatorial stratospheric cooling can also occur as a result of these events. Mechanisms responsible for the downward propagation of stratospheric anomalies have been summarized in previous studies by Tripathi et al. (2015) and Kidston et al. (2015).

The northern hemisphere annular mode (NAM) is a commonly used measure for assessing stratosphere-troposphere coupling during SSW events. Baldwin and Dunkerton (2001), for example, computed NAM indices from weak and strong vortex composites and observed that these events are often followed by the Arctic Oscillation (AO) pattern at the surface, which can persist for up to two months. The stratospheric anomaly propagating downward has numerous consequences for tropospheric weather, including shifts in storm track locations, changes in the likelihood and intensity of mid-latitude storms, variations in the frequency of high-latitude blocking events, and the occurrence of cold air outbreaks across the hemisphere (Thompson & Wallace, 2001). However, it is worth noting that not all SSW events result in a systematic tropospheric response, and the same is true for final stratospheric warming (FSW) events (Butler & Domeisen, 2021). Therefore, there has been ongoing research in the scientific community to classify SSW and FSW events and understand the factors that determine their different impacts on tropospheric circulation.

Traditionally, extreme SSW events have been classified as major based on the reversal of westerly winds at 10hPa-60°N (Butler et al., 2015). However, this criterion alone does not indicate whether an SSW event propagates downward. Other studies have classified SSW events based on the geometry of the polar vortex, distinguishing between displaced and splitting types (Charlton & Polvani, 2007; Cohen & Jones, 2011; Mitchell et al., 2013). Mitchell et al. (2013) found that splitting types tend to propagate downward, although this trend was not consistently observed in the study by Charlton and Polvani (2007), and exceptions exist, such as the SSW events observed in the winter of 1998/1999 (Baldwin & Dunkerton, 2001). Nevertheless, this finding aligns with the observations of Nakagawa and Yamazaki (2006), as displacement and splitting types are generally associated with upward fluxes of wavenumbers 1 and 2, respectively. However, the role of wave-1 activity is also significant in the occurrence of SSW events (Nakagawa & Yamazaki, 2006; Bancalá et al., 2012; Barriopedro & Calvo, 2014), and similar downward impacts can occur after both wave-1 and wave-2 SSW events, as seen in the SSWs of January 2009 (wave-2 type) and January 2010 (wave-1 type) (Ayarzagüena et al., 2011; Kodera et al., 2015).

While some studies have directly classified SSWs based on their tropospheric responses, such as absorbing or reflecting types (Kodera et al., 2016), the persistence of stratospheric anomalies (Runde et al., 2016), or surface observations of the North Atlantic Oscillation (Domeisen, 2019)and North Atlantic storm track response (Afargan-Gerstman & Domeisen, 2020), there are significant dissimilarities between these classifications in terms of identifying which SSW events have a descending effect (Karpechko et al., 2017) (see Table 1). Furthermore, Runde et al. (2016) found that 20% of extreme stratospheric events, including both strong and weak vortex events, resulted in a surface response, indicating that the mechanism responsible for the descending effect is still unclear, although anomalies in the lower stratosphere seem to play a crucial role.

On the other hand, FSW events have been classified based on their timing and nature, distinguishing between "early" and "dynamical" or "late" and "radiative" events (Waugh & Rong, 2002; Hauchecorne et al., 2022). The occurrence mechanism between mid-SSWs and early dynamical FSWs, both driven by waves, is similar (Vargin et al., 2020). Butler and Domeisen (2021) classified FSW events in both the northern and southern hemispheres based on dominant zonal wavenumber, timings, and their respective downward impacts. Interestingly, in the northern hemisphere, wave-2 events are followed by anomalously positive 500 hPa height anomalies over the North Pacific and the U.S., in contrast to wave-1 events, although the negative AO pattern remains consistent.

Recently, Mariaccia, Keckhut, and Hauchecorne (2022) proposed a new classification based on empirical orthogonal functions of stratospheric zonal wind fluctuation patterns at the edge of the polar vortex. Their study revealed four scenarios modulated by the timings and dynamical activities of important SSWs (ISSWs) occurring in mid-winter, along with scenarios without ISSWs but differing in the type of FSW (dynamical and early or radiative and late). This novel classification focuses on the entire winter evolution rather than specific SSW or FSW events, and it establishes a connection between mid-winter and winter end, highlighting the existence of a stratospheric memory as previously highlighted by Hauchecorne et al. (2022).

The primary objectives of this study are twofold: first, to demonstrate that this classification represents not only the unfolding of wintertime stratospheric circulation at the edge of the polar vortex but also the overall influence of northern hemisphere stratospheric evolutions on the troposphere during winter, and second, to investigate how stratospheric anomalies descend into the troposphere and manifest as surface signals throughout the winter season in the northern hemisphere. Additionally, the study aims to identify potential precursors at the surface in the months leading up to significant stratospheric anomalies, which could provide insights for seasonal predictability.

The structure of the paper is organized as follows. Section 2 presents the data extraction process from the ERA5 product, as well as the methods used to compute the NAM indices and the divergence of Eliassen-Palm flux in the stratosphere-troposphere. Section 3 describes the four scenarios and their respective dynamical characteristics. Sections 4 and 5 provide an analysis of NAM evolutions and surface impacts for the perturbed and unperturbed scenarios. Then, the impacts on surface temperature in early and late winter are examined in Section 6. Finally, Section 7 presents the summary and conclusions of the study, along with a discussion of its implications for seasonal predictability and future research directions.

2 Data and Method

2.1 ERA5 reanalysis

Since 2016, the European Centre for Medium-Range Weather Forecasts (ECMWF) has been generating a state-of-the-art reanalysis dataset called ERA5. This new generation of reanalysis benefits from the updated ECMWF Integrated Forecast System Cycle 41r2, which incorporates improved model parameterizations of convection and microphysics (Hersbach et al., 2020). ERA5 provides hourly output on a 0.25° latitude-longitude grid, with 137 vertical levels extending from the surface up to a pressure level of 0.01 hPa (approximately 80 km). As a result, ERA5 offers the longest reanalysis series available, spanning from 1940 to the present.

Recent studies have demonstrated that ERA5 temperature reanalysis accurately reproduces observed temperatures and their variability within the upper stratosphere during winter (Marlton et al., 2021; Mariaccia, Keckhut, Hauchecorne, Claud, et al., 2022). However, the mesosphere is not as well represented in ERA5. Consequently, the ERA5 dataset is particularly suitable for studying stratosphere-troposphere coupling over decades, specifically during the winter season.

ERA5 data is also readily available at 37 pressure levels, covering the entire troposphere-stratosphere region from 1000 to 1 hPa, with 11 additional levels between 100 and 1 hPa. For our analysis, we extracted the daily variables required to compute the Northern Annular Mode (NAM) indices and Eliassen-Palm flux from ERA5 reanalysis data at these pressure levels. Our analysis covers the grid from 20°N poleward and spans from 1950 to 2020, encompassing a total of 70 winters. The winter season in our analysis starts on November 1st and concludes on May 1st, spanning a period of 182 days.

2.2 Calculating the NAM indices

The Northern Annular Mode (NAM), also known as the North Atlantic Oscillation, is a key measure of dynamic variability during the winter season. It is computed by determining the leading empirical orthogonal function (EOF) that captures the dominant patterns of variability. The computation of NAM indices enables us to assess the influence of stratospheric variability on the spatial patterns observed in the troposphere.

Several methods exist for computing NAM indices, including surface-based EOFs, height-dependent EOFs, and zonal-mean EOFs. Each method has its advantages and drawbacks. The first two methods have limitations in capturing realistic annular variability in the middle atmosphere, as well as computational costs. In contrast, the zonal-mean EOFs method, as described by Baldwin and Thompson (2009), based on daily averaged, zonally averaged, year-round geopotential height, consistently captures annular variability structures and is employed in this study.

To calculate the daily NAM indices (y_l^d), the following equation is used:

$$y_l^d = \frac{\overline{Z_l^d} W e_l}{(e_l)^T W e_l}, \tag{1}$$

where $\bar{Z}_l^d$ represents the zonal mean of the daily geopotential anomaly, W is a vector used to spatially weight the NAM indices (cosine of latitudes), and e_l denotes the leading EOF of all zonal mean daily geopotential anomalies. Thus, we computed NAM indices for the 70 winters spanning from 1950 to 2020 using Equation 1. Subsequently, we averaged the daily NAM indices over the winters associated with each mode to obtain the mean time-height development of the northern annular mode.

By applying this approach, we can analyze the behavior of the NAM and its link to stratospheric variability, providing valuable insights into the stratosphere-troposphere coupling over the winter season.

2.3 Student's t-test

To assess the significance of the mean NAM indices and anomalies at 1000 hPa for each scenario, Student's t-tests were conducted. For the mean NAM indices, the null hypothesis of the t-test states that the means of the datasets are equal to the mean NAM indices observed over the 70 winters. On the other hand, for anomalies at 1000 hPa, the null hypothesis assumes that the means of the datasets are equal to zero. By performing these t-tests, we can determine whether the observed differences in the mean NAM indices and anomalies are statistically significant.

2.4 The divergence of Eliassen-Palm flux

The Eliassen-Palm (EP) flux is a vector that characterizes the direction of small atmospheric waves as well as the magnitude of eddy heat flux and momentum flux. It serves as a valuable diagnostic tool for investigating wave-mean flow interactions and, consequently, the coupling between the stratosphere and troposphere. The divergence of the EP flux provides information about the acceleration or deceleration of the zonal mean zonal wind.

In this study, ERA5 data has been extracted onto pressure levels and latitude degrees, and the divergence of the EP flux is computed using the methodology described by Jucker (2021). This approach accounts for spherical geometry, the aspect ratio of the figures, and the units of the vector components. The components of the EP flux in pressure coordinates are calculated using the equations introduced by Andrews et al. (1983):

$$f_\phi = -\overline{u'v'} + \overline{u}_p \frac{\overline{v'\theta'}}{\bar{\theta}_p}, \tag{2}$$

$$f_p = \left(f - \frac{1}{a\cos\phi} \frac{\partial(\bar{u}\cos\phi)}{\partial\phi} \right) \frac{\overline{v'\theta'}}{\bar{\theta}_p} - \overline{u'\omega'}, \tag{3}$$

where the notation follows the conventional usage, and primes and overbars represent perturbations and zonal means, respectively. Subscripts ϕ and p refer to partial derivatives with respect to latitudes and pressure levels. f denotes the Coriolis parameter, and a represents the radius of the Earth. The unit of f_ϕ is m^2/s^2, and assuming pressure is in hPa, f_p is in $m \cdot hPa/s^2$. To obtain the natural form of divergence on the (ϕ, p) plane, it is necessary to express the EP flux components in the scale units for ϕ and p on the diagram, as outlined by Edmon et al. (1980):

$$\mathbf{F} = \left(\hat{F}_\phi, \hat{F}_p\right) = \frac{2\pi}{g} a^2 \cos^2\phi \left(f_\phi, a f_p\right). \tag{4}$$

where $\mathbf{F}$ represents the EP flux components in the desired scale units. Finally, the mass-weighted divergence of $\mathbf{F}$ is simply given by $\partial_\phi \hat{F}_\phi + \partial_p \hat{F}_p$ and is expressed in units of m^3. In this study, the anomaly of EP flux divergence is computed daily for each winter on all pressure levels throughout the analyzed period. The mean divergence anomalies associated with the four different scenarios are presented in the subsequent section. The contributions of wave-1 and wave-2 to the mean divergence anomaly for each scenario are also calculated and can be found in the appendix section. However, a detailed discussion of their contributions will be provided in the following section.

3 The Dynamics of the Four Vortex Scenarios

A recent study by Mariaccia, Keckhut, and Hauchecorne (2022) classified 61 out of the 70 winters between 1950 and 2020 into four scenarios representing typical polar vortex evolutions. These scenarios include the January mode (17 winters), the February mode (17 winters), the Double mode (seven winters), and the unperturbed polar vortex evolution consisting of the Dynamical Final Warming (DFW) mode (15 winters) and the Radiative Final Warming (RFW) mode (five winters). The complete list of winters associated with each scenario can be found in Mariaccia, Keckhut, and Hauchecorne (2022). For the remainder of this study, we will focus separately on the DFW and RFW modes. Mariaccia, Keckhut, and Hauchecorne (2022) also found that each scenario exhibits distinct wave-1 and wave-2 activities in the middle stratosphere, consistent with zonal wind patterns over the winter months. However, as this investigation focused on a specific point in the northern hemisphere stratosphere (10 hPa and 60°N), further analysis is needed to confirm these trends at other altitudes and latitudes near the polar vortex edge.

To better understand the interaction between waves and the mean flow, we calculated the mean mass-weighted divergence anomaly of Eliassen-Palm flux for winters associated with perturbed and unperturbed scenarios. Figures 1 and 2 in this study show the divergence anomalies for perturbed and unperturbed scenarios, respectively. The wave-1 and wave-2 contributions to this divergence are provided in the appendix (Figures A1 and A2). We also examined the zonal mean zonal wind and temperature evolutions between 50°N and 70°N at 10 hPa to assess the effects of the EP flux divergence. These zonal mean evolutions closely resemble those reported by Mariaccia, Keckhut, and Hauchecorne (2022) at 60°N-10 hPa, confirming that the typologies identified in the northern hemisphere stratosphere are widespread.

In terms of the divergence patterns, significant signals are primarily observed in the upper stratosphere, where planetary waves break and deposit their momentum. As expected, we find that negative (positive) divergence values align with the deceleration (acceleration) of zonal winds and temperature increase (decrease) associated with SSWs and FSWs (polar vortex reinforcements). These results confirm the role of wave-mean flow interactions in weakening the zonal stratospheric circulation and warming the stratosphere. The magnitude and vertical extension of the divergence signal are likely responsible for the abrupt zonal wind deceleration observed at 10 hPa, with the February mode exhibiting a stronger wind deceleration gradient due to a negative divergence signal extending into the lower stratosphere. Interestingly, the divergence anomaly evolutions at 1000 hPa tend to herald the current or future signs of those in the upper stratosphere. These signals constitute a first attestation of the probable existent influences on the stratospheric dynamics by the surface climate.

In contrast, the divergences associated with the DFW and RFW modes display frequent oscillations between positive and negative values in the upper stratosphere over winter. These oscillations, accompanied by momentum and heat flux depositions on short time scales, are likely the reasons why winters in these modes remain unperturbed. Thus, it appears that longer periods of wave-mean flow interactions generating momentum and heat flux, as observed in the perturbed scenarios, are necessary to have a significant impact on the stratospheric circulation.

The contributions of wave-1 and wave-2 to the divergence evolutions align with the wave activity analysis performed by Mariaccia, Keckhut, and Hauchecorne (2022) for each scenario. The January and Double modes are predominantly driven by wave-1, while the February mode exhibits contributions from both wave-1 and wave-2. However, an interesting exception is observed in the DFW mode in December, where wave-1 accelerates the mean flow while wave-2 decelerates it. In the perturbed modes, wave-2 activity only influences the acceleration of the mean flow in the January and Double modes, whereas the opposite is true for the February mode.

These new findings further support the previously reported dynamical behaviors and enhance our understanding of wave activities in different scenarios and their impacts on polar vortex evolutions. However, since the mean divergence anomaly signals are primarily located in the upper stratosphere, it is challenging to infer how momentum and heat flux anomalies affect the troposphere. Therefore, in the next section, we investigate the troposphere-stratosphere coupling by examining the NAM evolutions for each scenario.

4 Perturbed Vortex Scenarios

4.1 NAM evolutions

Figure 3 illustrates the mean time-height evolution of the NAM indices calculated in the troposphere and stratosphere for the three perturbed scenarios: January, February, and Double modes. The figure includes solid black contour lines to indicate significant anomalies based on the Student's t-test. Weak and warm polar vortex periods are depicted in red, while strong and cold polar vortex periods are shown in blue. These findings align with previous studies, which have established that anomalies in the stratosphere exhibit longer time scales compared to fluctuations in the troposphere. Additionally, anomalies tend to first appear in the upper stratosphere before descending downward (Baldwin & Dunkerton, 2001; Mitchell et al., 2013). Furthermore, anomalies reaching the lower stratosphere tend to persist longer than those in the upper stratosphere due to the extended radiative time scale. Notably, strong anomalies located just above the tropopause have a higher tendency to propagate into the troposphere, underscoring the significance of this factor in the downward mechanism. Importantly, these NAM evolutions are consistent with the divergence evolutions of EP flux for the perturbed scenarios (see Figure 1).

For the January mode, an instantaneous and significant positive anomaly associated with weak polar vortex events caused by an ISSW emerges at the end of December. This

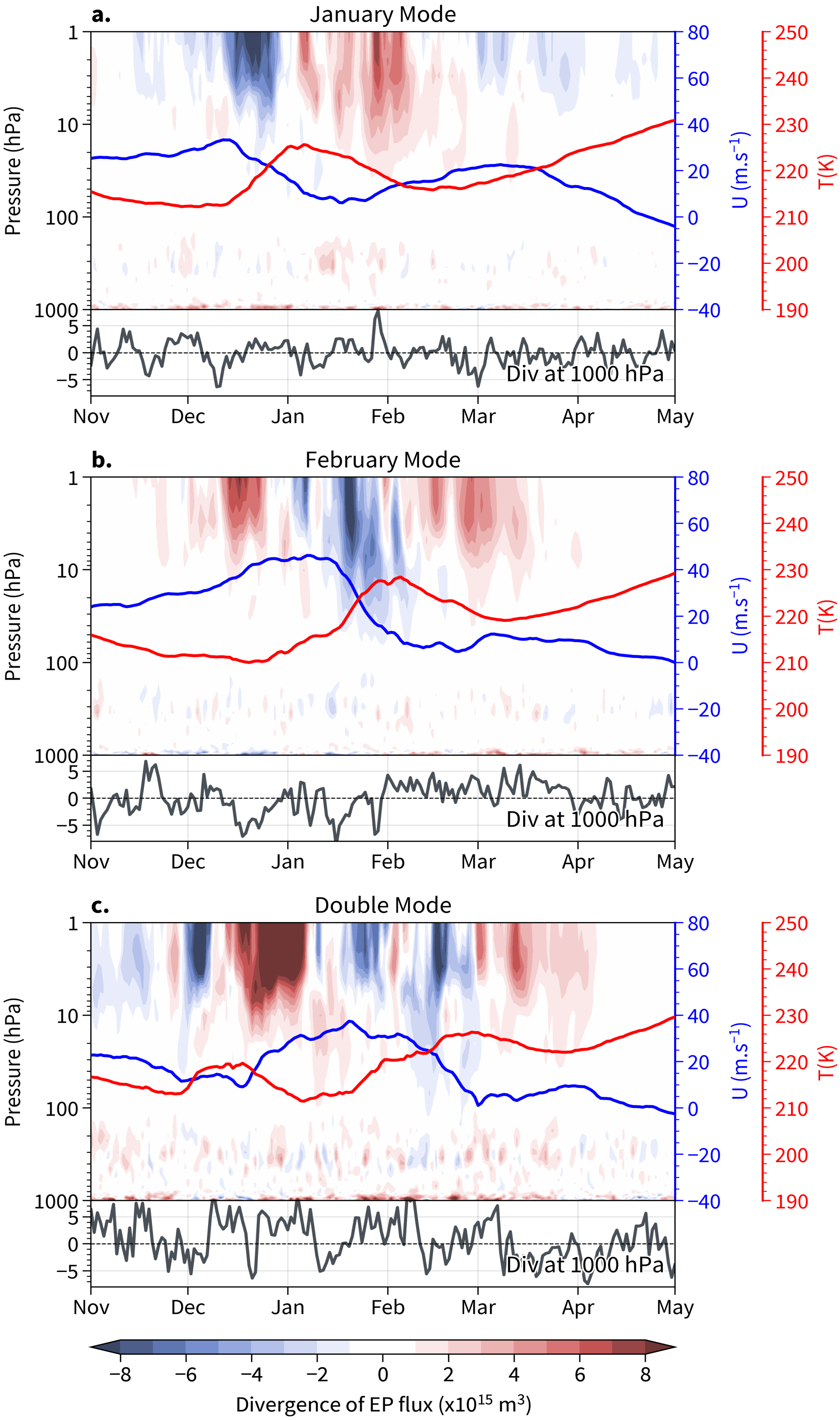

Figure 1. Mean time-height development of the anomaly of the mass-weighted divergence of Eliassen-Palm flux between 50 and 70°N for the three perturbed scenarios: the January Mode (a), the February Mode (b), and the Double Mode (c). Shaded negative (blue) and positive (red) values correspond to a deceleration and acceleration of the zonal wind, respectively. The panel at the bottom shows the evolution at 1000 hPa. Solid blue and red lines represent mean evolution of zonal mean zonal wind and zonal mean temperature, respectively, computed over the latitude range 50-70°N at 10 hPa.

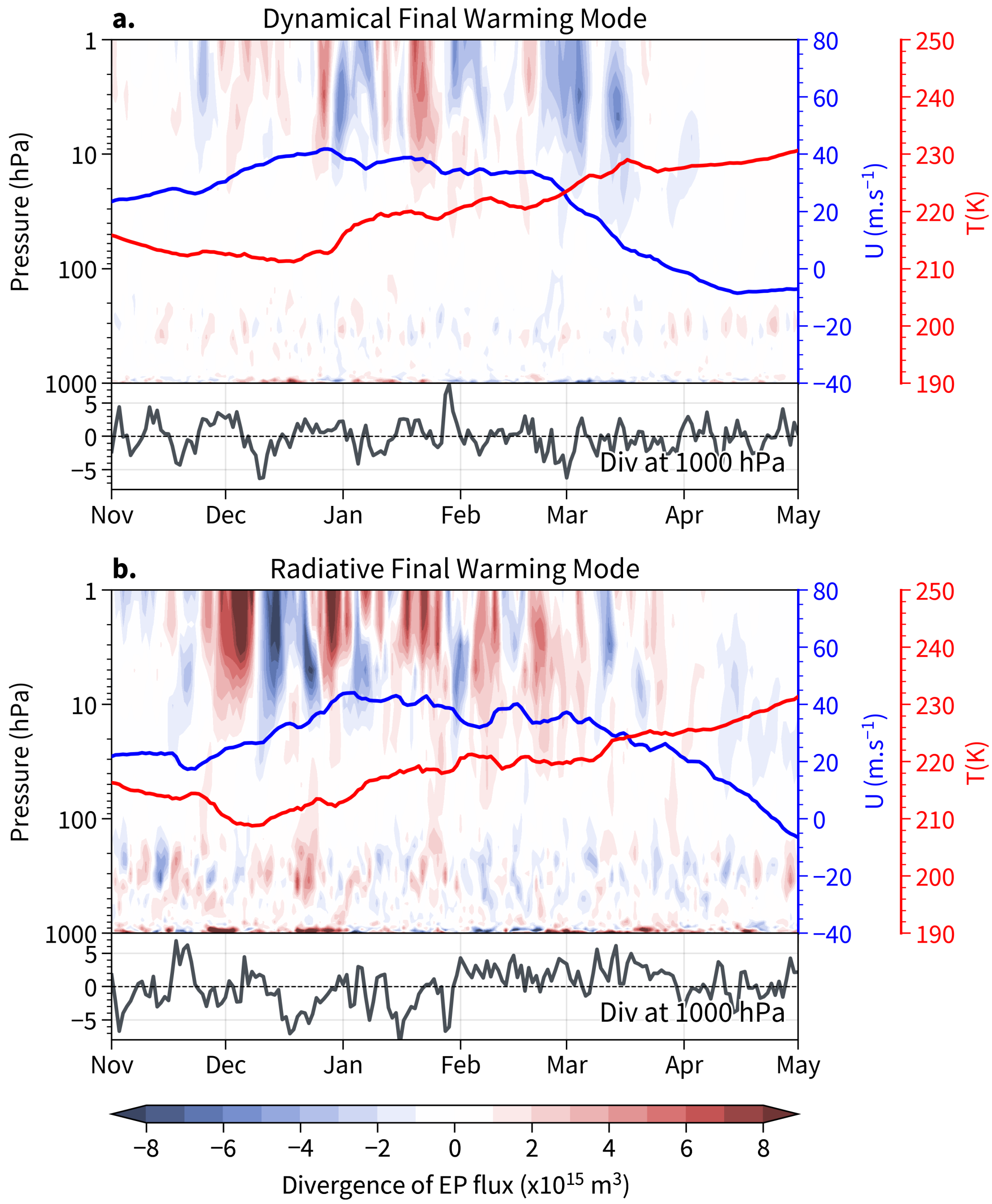

Figure 2. Mean time-height development of the anomaly of the mass-weighted divergence of Eliassen-Palm flux between 50 and 70°N for the two sub-modes composing the unperturbed scenario: the Dynamical Final Warming Mode (a) and the Radiative Final Warming Mode (b). Shaded negative (blue) and positive (red) values correspond to a deceleration and acceleration of the zonal wind, respectively. The panel at the bottom shows the evolution at 1000 hPa. Solid blue and red lines represent mean evolution of zonal mean zonal wind and zonal mean temperature, respectively, computed over the latitude range 50-70°N at 10 hPa.

anomaly rapidly propagates throughout the stratosphere with high significance from December to January. It covers the entire stratosphere and subsequently moves downward into the troposphere, reaching the Earth's surface significantly in January. From February, the positive anomaly begins descending from the upper to lower stratosphere, with a slight rise from the tropopause, halting the propagation into the troposphere. Another noteworthy positive anomaly at the surface emerges in late March, potentially representing a late tropospheric response to the strong positive anomaly that concluded in March. Simultaneously, a weak negative anomaly appears in the upper stratosphere, propagating downward to reach the lower stratosphere in April, without extending into the troposphere. The FSW, which commonly occurs around April 20th (Mariaccia, Keckhut, & Hauchecorne, 2022), does not induce a strong signal in the stratosphere or troposphere. Thus, these results align with the typical winter evolutions associated with this scenario, characterized by ISSWs in mid-January, followed by a weak reinforcement of the polar vortex in March before concluding in April. It is worth noting that, on average, no stratospheric anomaly precedes the positive anomaly associated with the ISSW's appearance at the end of December. This absence of an anomaly is attributable to the similarity in the seasonal wave activity cycle up to mid-December for most winters (Mariaccia, Keckhut, & Hauchecorne, 2022), resulting in a zero anomaly in the stratosphere at the beginning of winter. Beyond mid-December, the mean wave activity associated with the scenarios begins to diverge.

In the case of the February mode, a significant negative anomaly indicating strong polar vortex events instantaneously emerges and covers the entire stratosphere from mid-December to the end of January. Importantly, as this anomaly descends further toward the tropopause, it begins to significantly impact the troposphere, confirming the importance of this factor once again. Subsequently, a positive anomaly primarily appears in the upper stratosphere at the end of January, with a tilted descending phase that later reaches the lower stratosphere, lasting until April. However, no significant descent into the troposphere is observed since the positive anomaly remains predominantly above 100 hPa, which is too high to affect the tropopause and enable downward propagation. Nevertheless, positive anomaly signals, albeit not significant, emerge at the surface in March, suggesting a weak tropospheric response to this stratospheric anomaly on average. From March onward, a weak negative anomaly signal develops in the upper stratosphere, descending to the lower stratosphere, indicating the final formation of the polar vortex with weak winds before the occurrence of the FSW, often characterized by late and radiative events. Similar to the January mode, no significant anomaly precedes the negative anomaly in December in the stratosphere, as explained earlier. Therefore, these findings align with the mean zonal evolution associated with the February mode, featuring a stratospheric circulation reinforcement in December and January, followed by a rapid zonal wind deceleration due to an ISSW occurring at the end of January, before a radiative FSW at the end of April.

Lastly, winters associated with the Double mode exhibit, on average, a positive anomaly in the troposphere from mid-November. Surprisingly, unlike the January and February modes, this anomaly appears to propagate upward from the surface and precedes another positive anomaly covering the entire stratosphere from mid-December, corresponding to the first ISSW's occurrence. This upward propagation suggests that the positive anomaly at the surface acts as a tropospheric precursor to the subsequent ISSW's appearance. Hence, this anomaly propagation exemplifies the bidirectional stratospheric-tropospheric dynamical coupling and its potential usefulness for seasonal-scale climate forecasts. The positive anomaly descends into the lower stratosphere and propagates into the troposphere from mid-January. Concurrently, a negative anomaly emerges in the upper stratosphere from the beginning of January, descending to the lower stratosphere by early February, indicating the reformation of the polar vortex. Starting from mid-February, a new positive anomaly emerges, covering both the stratosphere and troposphere until the end of March. Interestingly, the maximum positive anomaly is observed at low altitudes around 200 hPa, corresponding to the second ISSW's occurrence. Thus, similar to the previous two modes, these findings align with the unfolding of mean stratospheric winter circulation and wave activity for the Double mode (see Figure 1), featuring an initial ISSW in December, a subsequent one around the end of February, and a vortex restoration between the two. In April, a negative anomaly begins to develop in the upper stratosphere, corresponding to a tentative restoration of the polar vortex, which is interrupted by the FSW, often characterized by late and radiative events during this period. The absence of propagation of this negative anomaly suggests that the presence of tropospheric anomalies is unrelated.

In conclusion, these mean time-height evolutions of NAM indices indicate that these three perturbed scenarios possess distinct vertical structures influenced by the timings of ISSWs and FSWs. On the whole, positive anomalies generated by ISSWs tend to propagate downward into the troposphere immediately or with a delay of one month after their occurrence. However, this behavior is not observed for FSWs, which are mostly radiative and do not tend to impact the troposphere significantly. Notably, both the stratosphere and troposphere exhibit weak signals in April. These findings affirm that the new classification determined in Mariaccia, Keckhut, and Hauchecorne (2022) not only represents different stratospheric wind scenarios but also repetitive typical spatial patterns that couple the stratosphere with the troposphere during Northern Hemisphere winters. In the next section, we will discuss the probable polar vortex geometry associated with these perturbed scenarios by comparing with the classification performed in Mitchell et al. (2013). Then, we will investigate the surface regions impacted in the Northern Hemisphere over the months for these three perturbed scenarios.

4.2 Link With Horizontal Polar Vortex Geometry

The propagation of instantaneous anomalies throughout the stratosphere and troposphere after ISSWs in the January mode bears resemblance to the findings of Splitting events in Mitchell et al. (2013) (see Figure 4b), suggesting a potential wave resonance phenomenon caused by barotropic mode excitation (Esler & Scott, 2005). Thus, one might expect the January mode to be associated with splitting polar vortex evolutions. However, this concurrence is surprising since the January mode is primarily driven by wave-1 activity, usually characterized by displaced events. Similarly unexpected, the tilted downward propagation observed in the stratosphere for the February mode aligns with the findings for Displacement events in Mitchell et al. (2013) (see Figure 4a), showing limited impacts in the troposphere. This result is also surprising as the February mode exhibits strong wave-2 activity, typically associated with splitting events. Moreover, this result is consistent with the seasonal distribution of splitting, displacement, and mixed events presented in Mitchell et al. (2013) (see Figure 3), where splitting events are more concentrated in December and January, while displaced events occur more frequently in February and March. However, it should be noted that this distribution differs from that obtained by Charlton and Polvani (2007), who used a different method to identify polar vortex geometry during SSWs. This discrepancy highlights the importance of considering methodological uncertainties when comparing these classifications. Hence, despite these seemingly contradictory findings, all inferences drawn from this comparison are likely irrelevant. The primary reason is that the established scenarios are not based on specific SSW dates but rather on winter typologies, representing a novel approach that hampers direct comparisons with such classifications. Furthermore, even previous SSW classifications exhibit contradictions and divergences in identifying the mechanism responsible for downward effects into the troposphere (Karpechko et al., 2017), necessitating further clarification. Additionally, most studies, including the NAM evolutions presented here, argue that the persistence of circulation anomalies in the lower stratosphere plays a crucial role in this process. Consequently, without making assumptions with significant uncertainties, it is impossible to draw conclusions regarding the vortex geometry associated with these perturbed scenarios. Nonetheless, this feature appears to be less decisive than the timing of ISSWs in predicting stratospheric anomaly descents and surface impacts.

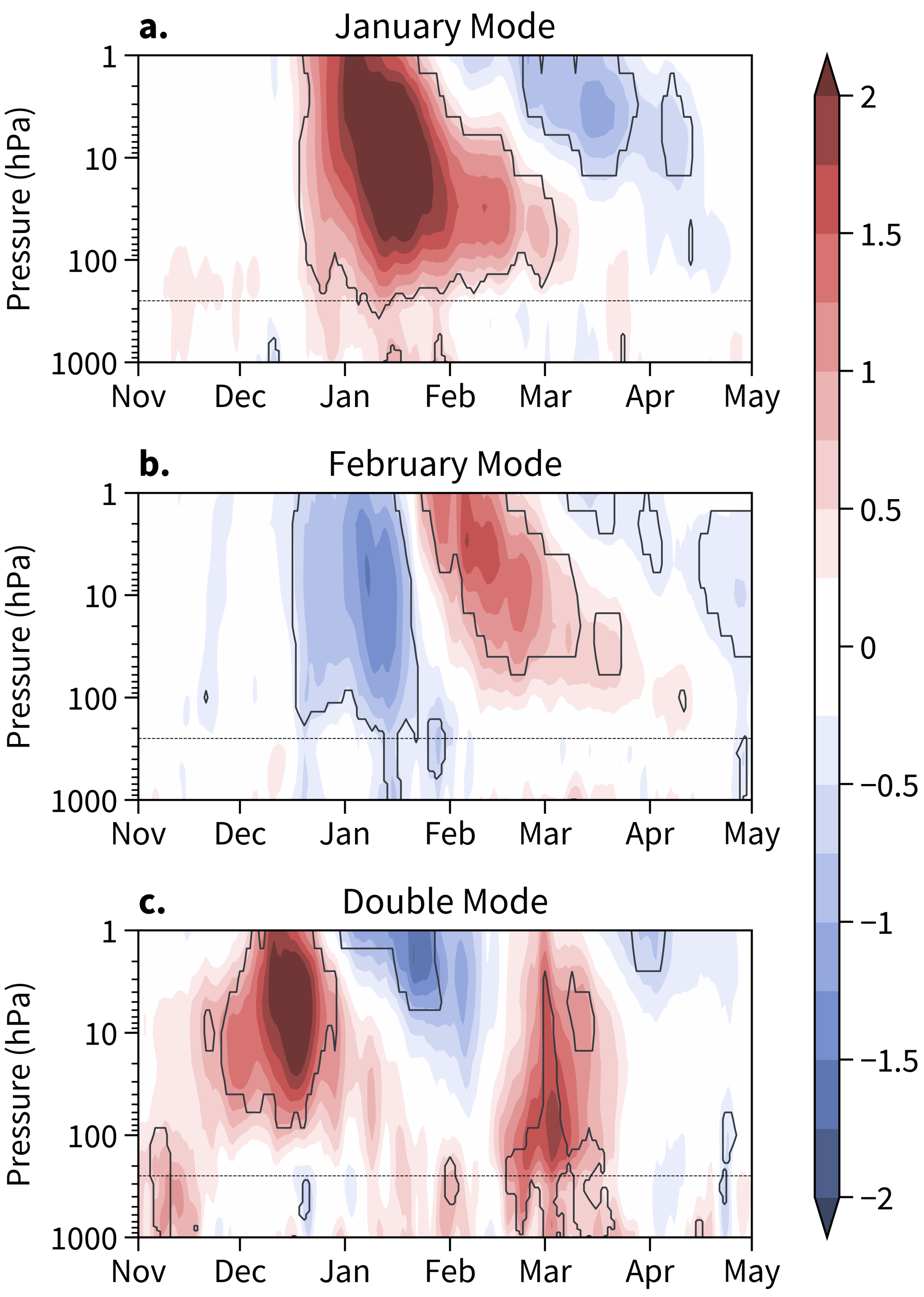

Figure 3. Mean time-height development of the northern annular mode indices for the winters associated with the three perturbed scenarios: the January Mode (a), the February Mode (b), and the Double Mode (c). The indices have daily resolution and are non-dimensional. Negative values (blue) corresponds to a strong polar vortex and positive values (red) to a weak polar vortex. The black lines contour areas with statistical significance at the 95% level according to a Student's t test. The horizontal black dashed lines indicate the approximate delimitation between the troposphere and the stratosphere.

4.3 Surface impacts at 1000 hPa

Figure 4 illustrates the evolution of monthly mean geopotential anomalies at 1000 hPa for the three perturbed scenarios from November to March. The stippled areas indicate the regions of highest significance according to the Student's t-test.

For the January mode, it can be observed that winters begin in November with a few surface signals of high significance: a positive anomaly over the Barent Sea and a negative anomaly in Western Europe. In December, significant signals are found across the investigated area. Therefore, winters typically exhibit a geopotential dipole with strong positive anomalies over Siberia and Asia, while significant negative anomalies cover the center and Northwest America. Interestingly, these surface signals display a wave-1-like pattern, coinciding with significant wave-1 activity diagnosed in the middle stratosphere before the occurrence of ISSWs for the January mode (see Fig. 8a in Mariaccia, Keckhut, and Hauchecorne (2022)). Thus, these results suggest that the surface pattern observed in December acts as a precursor to a specific wave-1 activity propagating upward from the troposphere and disturbing the stratospheric circulation, which in turn impacts the surface in the following months. This connection exemplifies the two-way troposphere-stratosphere coupling that takes place in the northern hemisphere during winter. In January, which is when the ISSW is expected to occur for winters associated with this mode, strong positive anomalies are observed at the pole and eastern Siberia, while negative anomalies are found in southern Europe and Northeast America. This pattern is typical of the negative phase of the AO. It is consistent with the NAM indices showing a downward propagation of positive anomalies in January (see Fig. 3). The positive anomaly persists at the pole until March but exhibits a rotational motion over the months. In February, this positive anomaly signal extends further over northern Canada, while in March, it covers Iceland and a part of the Pacific, with an overall decrease in significance.

Regarding the February mode, surprisingly, opposite signals are observed compared to the January mode, particularly for the months from November to January, confirming that these two modes possess very different initial surface conditions. In November, winters tend to have a negative anomaly over the Barent Sea, while a positive anomaly, though not highly significant, is observed in Western Europe. In December, the previous negative anomaly covers a portion of Siberia, and another negative anomaly appears over the west of Greenland, while a positive anomaly is observed over the U.S. West Coast. Another positive anomaly is found over Western Europe but lacks high significance. Interestingly, this surface pattern exhibits a wave-2-like pattern, especially for the negative signals, aligning with the period when wave-2 activity in the stratosphere increases for this mode (see Fig. 8b in Mariaccia, Keckhut, and Hauchecorne (2022)). Therefore, similar to the January mode, this surface pattern serves as an indicator of a future weak polar vortex generated by an ISSW in February. More generally, these results support the idea that December is a crucial month for identifying and anticipating the occurring scenario. In January, a negative anomaly is present at the pole, while a positive anomaly is observed in western Europe, albeit with low significance. Again, this result aligns with the NAM indices computed for this mode, which indicate a descent of negative anomalies during this period. This pattern corresponds to the positive phase of the AO. As expected, no significant signals are found in February when the ISSW is expected to occur, confirming that the anomaly does not reach the surface. Only a small positive anomaly signal in the Bering Sea tends to be recurrent in February, albeit with significance. In March, only a negative anomaly is present over the north of the U.K., while a positive anomaly is found over Northeast America. Therefore, these weak surface signals following the ISSW confirm that the overall troposphere evolves somewhat independently from the stratosphere.

Unlike the January and February modes, the Double mode exhibits strong signals in November, with a positive anomaly over the pole and the Barent Sea, while negative anomalies cover southern Europe and the Bering Sea. This pattern shares similarities with the one observed in December for the January mode, i.e., a wave-1-like pattern that can

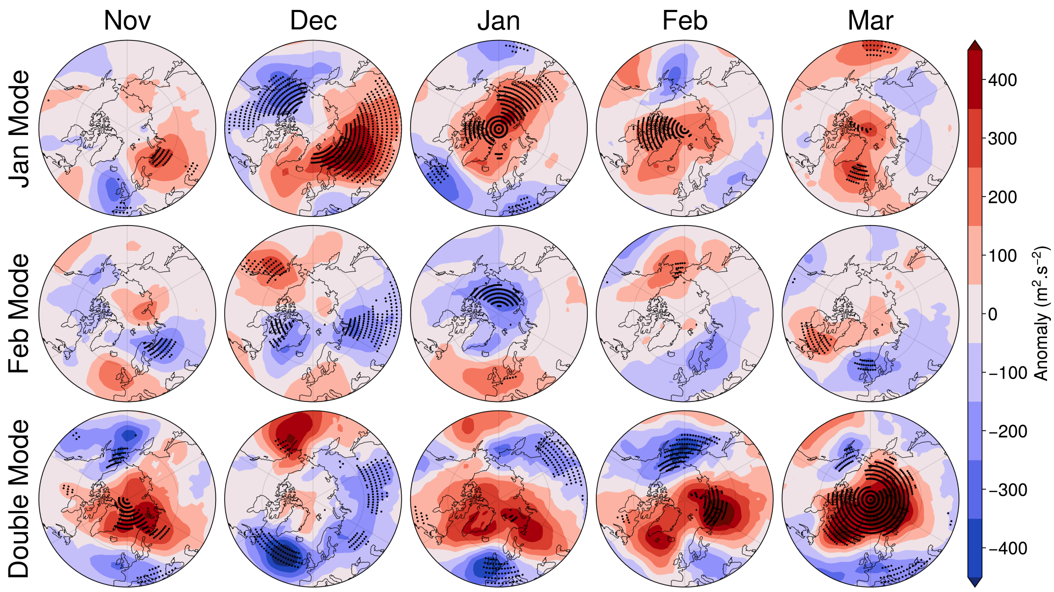

Figure 4. Monthly mean geopotential anomaly at 1000 hPa from 40°N poleward in the northern hemisphere for the three perturbed scenarios from November to March. Blue and red shaded regions respectively correspond to negative and positive geopotential anomalies. Stippled areas show statistical significance at the 95% level according to a Student's t test.

act as a precursor to the expected ISSW in the following month. In December, significant negative anomalies cover the North Atlantic Ocean and Eurasia, while a positive anomaly is present over the Bering Sea. Although the first ISSW occurs in December, there is no immediate downward propagation of the positive anomaly, as shown in Figure 3, where the descent into the troposphere occurs later in January and February. However, a significant positive anomaly is found in January, covering North America, the pole, and the land around the Barent Sea, albeit with low significance. Meanwhile, negative anomalies are present in Western Europe and China. In February, a significant positive anomaly over northern Siberia suggests that the stratospheric anomaly finally reached the surface. Simultaneously, a significant negative anomaly is present over the Bering Sea. Finally, in March, a negative phase of the AO is observed again due to the effect of the second ISSW, with a significant positive anomaly covering the entire pole, Greenland, and a northern part of Siberia.

Thus, based on Figure 4, it is evident that these three perturbed modes exhibit distinct surface signature evolutions throughout winters before and after the occurrences of ISSWs. However, there are similarities in the initial surface conditions and surface impacts between the January and Double modes, which are opposite to those observed for the February mode. Specifically, for the January and Double modes, a wave-1-like pattern is present at the surface in December and November, respectively, and the positive geopotential anomaly tends to propagate from the stratosphere to the surface after an ISSW, generally inducing a negative phase of the AO. In contrast, although the February mode displays a wave-2-like pattern at the surface in December, ISSWs occurring in February do not have subsequent impacts on the surface in the following months. Consequently, these perturbed scenarios exhibit precursors at the surface at the beginning of winter, particularly in December, which are likely responsible for the observed wave activity in the stratosphere and, therefore, appear crucial for anticipating the subsequent winter months. Regarding FSWs, their occurrence does not seem to significantly impact the surface, regardless of the perturbed mode. The investigation of the unperturbed mode and its two sub-modes, DFW and RFW, is presented in the next section.

5 Unperturbed Vortex Scenario

5.1 NAM evolutions

Figure 5 presents the NAM indices for the DFW and RFW modes, following a similar format to Figure 3. In line with expectations, both sub-modes exhibit a negative anomaly in the stratosphere, indicative of a persistent polar vortex that extends until the end of winter, finishing with either dynamical or radiative FSWs.

For the DFW mode, a negative anomaly forms on average in the stratosphere around 10 hPa starting in December. This negative anomaly propagates downward, gradually encompassing the entire stratosphere while intensifying until the end of February, reaching a peak around 30 hPa. The negative anomaly persists in the stratosphere until the end of February, at which point it initiates descent towards the troposphere, approaching the tropopause. Consequently, the negative anomalies reach the Earth's surface until the end of March. Interestingly, in early March, a positive anomaly appears at the top of the diagram. This positive anomaly corresponds to the occurrence of a dynamical FSW, which disrupts the polar vortex, resembling but with less intensity than the ISSWs observed in the three perturbed scenarios. Throughout March, this tilted positive anomaly propagates downward and reaches the lower stratosphere in April, but it does not significantly penetrate into the troposphere.

Regarding the RFW mode, weak but discernible anomaly signals are present in November, with a positive anomaly in the stratosphere and a negative anomaly in the troposphere. This positive anomaly descends while gaining strength, reaching the tropopause region and influencing the troposphere in December. Concurrently, a robust negative anomaly begins to form in the upper stratosphere. This negative anomaly propagates downward, covering the entire stratosphere from mid-January to mid-April while maintaining its intensity, indicating a persistently strong polar vortex throughout winter. From January to April, the tropospheric surface experiences the effects of this robust polar vortex, as anomalies persist just above the tropopause, facilitating their spread into the troposphere. It is important to note that this scenario represents the average evolution of only five winters, making this result statistically less robust than others. Notably, the surface is strongly influenced by the final stages of the wintertime stratospheric circulation in April, coinciding with the occurrence of the radiative FSW.

In the next section, we delve into the surface impact analysis for both sub-modes, examining the affected regions over the course of several months.

5.2 Surface impacts at 1000 hPa

Figure 6 illustrates the monthly mean geopotential anomaly at 1000 hPa from January to April for both the DFW and RFW modes. The decision to display only the months when stratospheric anomalies strongly impact the surface was made because undisturbed winters do not exhibit significant signals before January (not shown).

Regarding the DFW mode, significant anomalies are observed at the surface in February and March. In both months, a substantial negative anomaly is present at the pole and north of America, while a positive anomaly is observed in central Europe and northern Europe in February and March, respectively. Additionally, a notable negative anomaly tends to appear in the Pacific Ocean in March. Thus, these two months share a similar pattern, characteristic of a positive phase of the AO. The positive AO phase in the DFW mode is induced by a downward propagation of stratospheric anomalies, confirming their connection with strong polar vortex events. Furthermore, the surface signal in the DFW mode exhibits a wave-1-like pattern, consistent with the wave activity diagnosed in the stratosphere during this period (Mariaccia, Keckhut, & Hauchecorne, 2022), indicating a vertical connection from the surface to the upper stratosphere. This persistent wave-1 activity is likely the

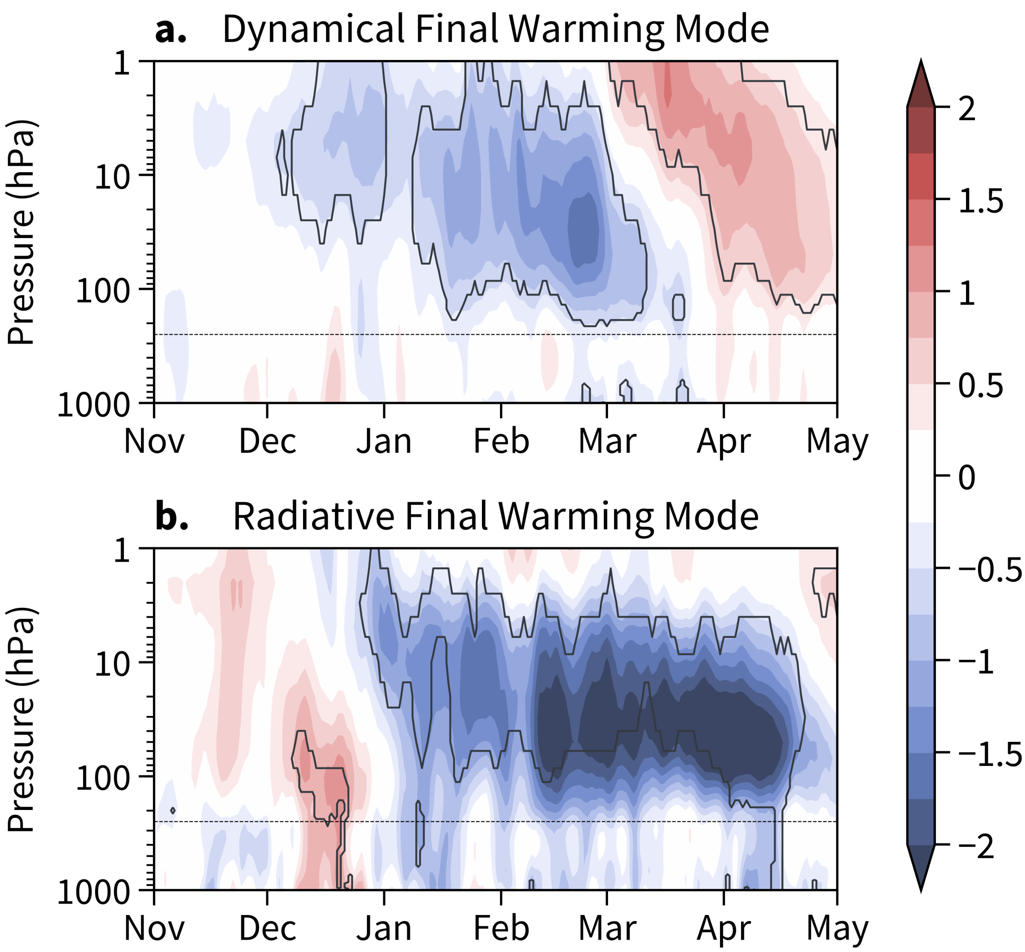

Figure 5. Mean time-height development of the northern annular mode indices for the winters associated with the two sub-modes composing the unperturbed scenario: the Dynamical Final Warming Mode (a) and the Radiative Final Warming Mode (b). The indices have daily resolution and are non-dimensional. Negative values (blue) corresponds to a strong polar vortex and positive values (red) to a weak polar vortex. The black lines contour areas with statistical significance at the 95% level according to a Student's t test. The horizontal black dashed lines indicate the approximate delimitation between the troposphere and the stratosphere.

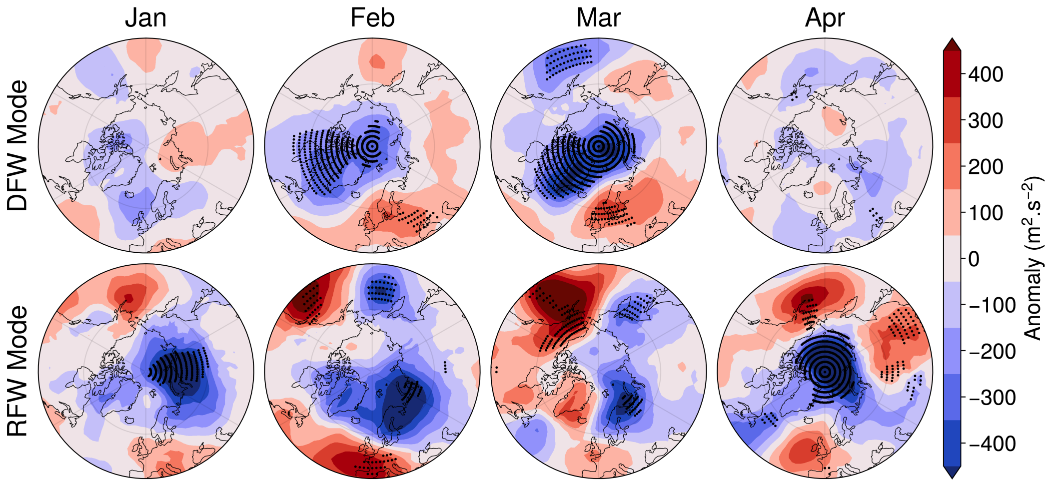

Figure 6. Monthly mean geopotential anomaly at 1000 hPa from 40°N poleward in the northern hemisphere for the two sub-modes composing the unperturbed scenario from November to March. Blue and red shaded regions respectively correspond to negative and positive geopotential anomalies. Stippled areas show statistical significance at the 95% level according to a Student's t test.

cause of the dynamical FSW occurring in April, similar to the disturbed scenarios. However, unlike wave-1-driven ISSWs, the final pattern in April is not influenced by the positive stratospheric anomaly generated by the dynamical FSW, as seen in the NAM evolution (see Fig. 5).

In contrast, the RFW mode shows significant signals throughout the studied period. In January, a highly significant negative anomaly is found from the pole to the north of Siberia, in agreement with the descending stratospheric anomaly during this period (see Fig. 5a). In February, the negative anomaly persists but with reduced significance, and an additional negative anomaly appears in the Pacific below the Bering Sea. Positive anomalies are observed in the Pacific near the U.S. west coast and in western Europe. In March, the preceding negative anomalies shift slightly to northern Europe and Russia's east coast, respectively, while the previous positive anomaly over western Europe diminishes, and the one in the Pacific moves westward and spreads over Alaska. The RFW mode's NAM evolution suggests that the surface patterns in February and March are less affected by the stratosphere due to the less significant descent of anomalies during these months.

Moreover, the surface signal in March exhibits a wave-2-like pattern that aligns with the peak of wave-2 activity found in the stratosphere during this period (Mariaccia, Keckhut, & Hauchecorne, 2022). This result confirms the vertical connection through wave activity when the polar vortex is strong, characterized by westerly winds that enable planetary wave propagation. However, despite significant wave-2 activity in March, there is no generation of stratospheric anomalies associated with triggering an ISSW, indicating the essential role of wave-1, which exhibits low activity during this period. In April, a strong and significant negative anomaly is found at the pole, while positive anomalies are observed over the Bering Sea and the center of Siberia and China. This pattern reflects a positive phase of the Arctic Oscillation, similar to what is found in February and March of the DFW mode. It aligns with the last observed anomaly descent in the NAM evolution. Beyond April, no further stratospheric anomalies are present due to the return of solar radiation, dissipating the polar vortex.

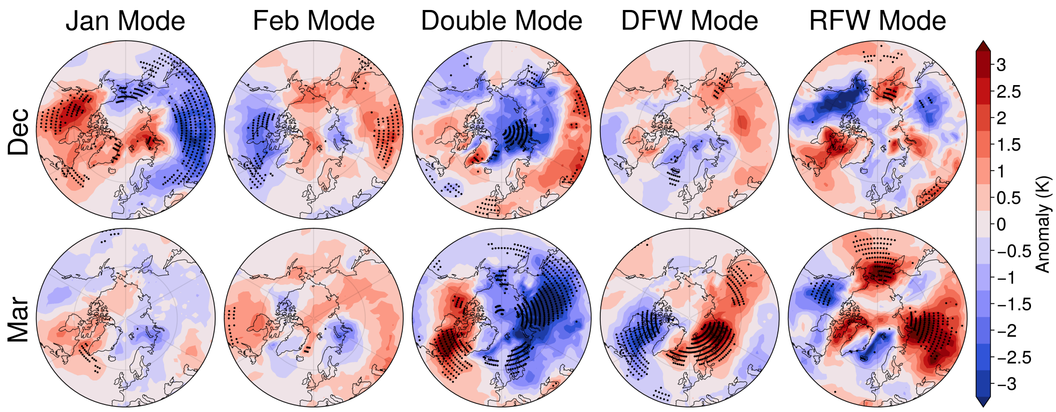

Figure 7. Monthly mean temperature anomaly at 1000 hPa from 40°N poleward in the northern hemisphere for each scenario in December and March. Stippled areas show statistical significance at the 95% level according to a Student's t test.

In summary, winters associated with the two sub-modes of the unperturbed scenario exhibit similar surface patterns significantly impacted by the downward propagation of negative stratospheric anomalies during the winter months. A positive Atlantic Oscillation emerges at the surface when the FSW occurs in both the DFW and RFW modes. These surface patterns differ notably from those obtained in the three perturbed scenarios, which are characterized by negative AO patterns after ISSWs. Therefore, the positive AO patterns observed in March and April for the DFW and RFW modes signify the disappearance of the polar vortex. This finding confirms that the timing and nature of FSWs are crucial for understanding the temporal shift in observed ground impacts. However, no significant surface harbingers are found in December and preceding months, suggesting that the FSW type is influenced more by January onwards rather than early winter.

6 Impacts on Surface Temperature

To investigate the effects of different scenarios on climate during winter, which is crucial for seasonal-scale weather forecasts, we present the monthly mean temperature anomaly at 1000 hPa in December and March in the northern hemisphere for each scenario (Fig. 7). Additionally, since the Double mode exhibits significant geopotential signals earlier in winter (Fig. 4), we also include the mean temperature anomaly at 1000 hPa in November for the Double mode in Figure 8. Generally, positive geopotential anomalies are associated with negative temperature anomalies, and negative geopotential anomalies are associated with positive temperature anomalies during the same period.

In December, it is not surprising to find that the January and February modes exhibit opposite dipole signals, consistent with the mean geopotential anomaly shown previously for this month. The January mode shows negative temperature anomalies ranging from -1 to -3 K over Eurasia, while positive anomalies of +1 to +2.5 K are observed over North America and Greenland. Notably, this temperature anomaly pattern over Eurasia in December bears similarities, but with higher significance, to the surface temperature anomalies found in the -30 to 0 days before Displacement Sudden Stratospheric Warming (SSW) events (Mitchell et al., 2013). In contrast, the February mode demonstrates less significant signals, with temperature anomalies only reaching +1.5 K in Siberia and -1.5 K in North America.

Interestingly, the mean temperature anomaly patterns observed in December and January (not shown here) for the February mode do not correspond to the precursor stage for either Displaced or Splitting events suggesting a mixed signal. Regarding the geopotential

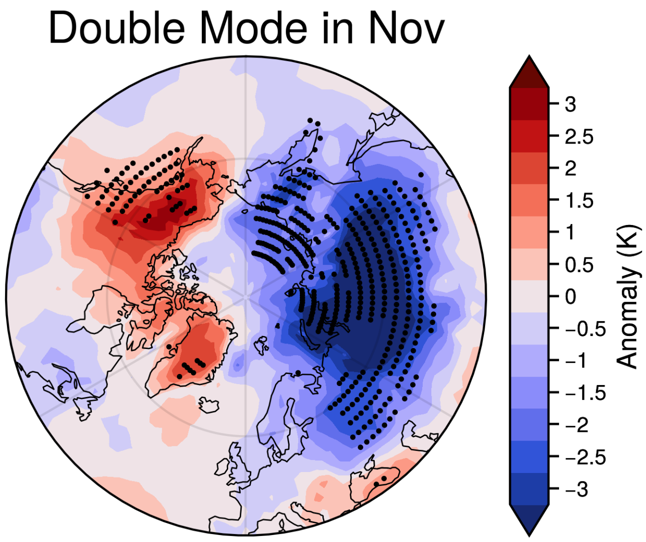

Figure 8. Monthly mean temperature anomaly at 1000 hPa from 40°N poleward in the northern hemisphere for the Double mode in November. Stippled areas show statistical significance at the 95% level according to a Student's t test.

anomaly, the temperature anomaly observed in November for the Double mode is similar to the one observed in December for the January mode, but with stronger negative anomalies over a large part of Eurasia exceeding -3 K, and positive anomalies of +1.5 K mainly covering North West America and Greenland. Despite the weak significance in December, the Double mode exhibits positive and negative temperature anomalies in the south and north of Siberia, respectively, indicating a warming of the Eurasia region when the first SSW of this scenario occurs in the stratosphere. These surface temperature patterns, similar to the geopotential patterns, can be considered precursors of these perturbed scenarios, providing further evidence that troposphere-stratosphere coupling substantially influences the winter climate in the northern hemisphere. These findings are of great interest for improving sub-to-seasonal forecasts. However, for the December month, the signals observed for the DFW and RFW modes have weak significance, consistent with the NAM evolution during this period. Therefore, the absence of surface signals with high significance up to December indicates that the winter is following an unperturbed scenario.

In March, the January and February modes exhibit similarities but do not show mean temperature anomalies with high significance, suggesting that the surface climate at this period is no longer influenced by stratospheric anomalies, which aligns with the observed NAM evolutions (Fig. 3a-b). Hence, surface precursors can anticipate these two scenarios in December, but they are not indicative of a specific surface climate at the end of winter. It is noteworthy that their surface patterns in March are similar to those observed for Splitting and Displacement events in their decay phase (Mitchell et al., 2013), making it challenging to draw meaningful comparisons or deductions.

Interestingly, the Double mode shows nearly identical surface signals in March as those observed in November, but with positive temperature anomalies covering a larger area in North East America exceeding +3 K. Thus, the surface harbinger found in November associated with the Double mode is similar to the effect generated by the second SSW occurring at the end of February. Consequently, the Double mode is a unique mode with a strong impact on the northern hemisphere's surface climate from November to March.

Finally, in March, the surface signals observed for the DFW and RFW modes are opposite to those found for the Double mode but similar to those observed in December for the February mode. The DFW mode shows a significant positive temperature anomaly exceeding +3 K over the Barent Sea region, ranging between 1 and 2 K in East Siberia, and negative anomalies averaging -1.5 K over North-East America. Similarly, the RFW mode exhibits positive anomalies exceeding +2.5 K on average over the center of Siberia and the Bering Sea region, while substantial negative temperature anomalies of -3 K and below are found over West America, Iceland, and Svalbard. Consequently, the similar temperature surface patterns between the DFW and RFW modes indicate that the type of final stratospheric warming does not determine a specific meteorological impact.

In general, these different surface harbingers and responses provide evidence for the existence of a connection between early and late winter due to stratosphere-troposphere coupling, confirming its significant influence on the climate in the northern hemisphere during wintertime.

7 Summary

In this study, we have conducted an investigation into the coupling between the stratosphere and troposphere for both perturbed and unperturbed scenarios, as established in a previous work by Mariaccia, Keckhut, and Hauchecorne (2022). By analyzing the time-height evolutions of the mass-weighted divergence anomaly of the Eliassen-Palm flux, averaged in the latitude range of 50-70°N, we have found that the mean eddy heat and momentum flux primarily influence the upper stratosphere. These findings are consistent with the zonal mean temperature and zonal mean zonal wind evolutions at 10 hPa within the same latitude range. In addtion, the divergence evolutions at 1000 hPa reveal that the dynamics in the upper stratosphere is potentially influenced by the surface some weeks in advance. Moreover, our analysis of the contributions from wave-1 and wave-2 to this divergence anomaly aligns with the wave activities associated with each scenario as reported earlier. Notably, we have observed that wave-2 plays a role in reinforcing the polar vortex following the occurrence of the ISSW for the January and Double modes.

Regarding the unperturbed scenario, we have identified frequent oscillations in the sign of the divergence in the upper stratosphere. These oscillations provide a physical explanation as to why the polar vortex remains strong during this scenario. These wave activity diagnoses enhance our understanding of the distinct dynamical behaviors exhibited by these scenarios and their impact on polar vortexes. Such inferences are crucial for potential simulations of these scenarios using mechanistic models.

We have also found that the time-height Northern Annular Mode (NAM) evolutions associated with each scenario align temporally with the phases of reinforcement and weakening of the polar vortex caused by ISSWs and FSWs. The discrepancies observed in these NAM evolutions, particularly in the descent of stratospheric anomalies caused by ISSWs or strong polar vortex events, provide confirmation that these scenarios affect the stratosphere and troposphere differently throughout the winter. Consequently, these novel findings offer compelling evidence of stratosphere-troposphere coupling during the winter months. Moreover, consistent with most studies, our results suggest that downward propagation toward the tropopause is crucial for enabling the descent of stratospheric anomalies to the surface, irrespective of their sign. In a broader sense, these outcomes verify that these scenarios not only represent a wind and temperature evolution at the edge of the polar vortex but also distinct states of the stratosphere and troposphere that influence each other during the winter months in the northern hemisphere. Overall, the diverse NAM evolutions demonstrate unique vertical and temporal connections in wintertime, which are of significant interest for climate forecasts.

When comparing our results with the classification based on vortex geometry, specifically displaced or splitting events, as performed by Mitchell et al. (2013), we have encountered inconsistencies between the NAM evolutions, surface temperature anomalies, and observed wave activity for perturbed scenarios. These discrepancies are likely attributed to the different approaches in the classifications, one based on the dates of SSW events and the other on main winter typologies, thereby hindering meaningful comparisons. Additionally, uncertainties exist in the method used to identify the polar vortex geometry. Consequently, establishing a direct relationship between a specific polar vortex geometry and each scenario based on this comparison is not evident. Thus, the timing of ISSWs appears to be more crucial than vortex geometry in attempting to predict a descent of stratospheric anomalies.

After examining the surface patterns of geopotential and temperature anomalies, several important findings emerge regarding the precursors and tropospheric responses during winter for each scenario:

1. January mode:
   - In December, there is a dipole structure of mean geopotential anomalies, with positive anomalies over Eurasia and negative anomalies over North-West America. This pattern is accompanied by mean temperature anomalies of -2 K over Eurasia and +2 K over North America. These surface patterns act as a precursor to the occurrence of an ISSW in January.
   - In January and February, a negative phase of the AO is observed at the surface due to the descent of positive stratospheric anomalies generated by the ISSW.
2. February mode:
   - In December, an opposite signal to the January mode is observed, with negative geopotential anomalies over Siberia and West Greenland, and positive anomalies over the U.S. West Coast. This surface signal exhibits a wave-2-like pattern, acting as a harbinger of the ISSW in February. Associated temperature anomalies reach, on average, +1.5 K over Siberia and -1.5 K over North America.
   - In January, a positive phase of AO appears at the surface due to the descent of negative stratospheric anomalies, indicating the presence of a strong polar vortex. From February onwards, no significant signals indicate that the stratosphere no longer influences the surface.
3. Double mode:
   - In November, the mean geopotential anomaly shows positive anomalies over the pole and the Barent Sea, and negative anomalies over southern western Europe and the Bering Sea. This signal shares similarities with the December pattern observed for the January mode. Associated with these anomalies are surface temperature anomalies exceeding -3 K over Eurasia and around +1.5 K over North West America and Greenland. These patterns exhibit a wave-1-like structure, acting as a precursor for the Double mode.
   - In January and February, the first ISSW causes the descent of the stratospheric anomaly into the troposphere. This leads to positive geopotential anomalies over Greenland and the Barent Sea, and negative anomalies over western Europe and China in January, and the Bering Sea in February.
   - In March, the second ISSW generates a significant descent of the stratospheric anomaly, resulting in a substantial negative AO phase. This is associated with temperature anomalies exceeding +3 K over North East America and -3 K over Eurasia.
4. DFW mode:
   - Consistent with its NAM evolution, no surface precursor exists for this mode, and no significant anomalies appear before February.

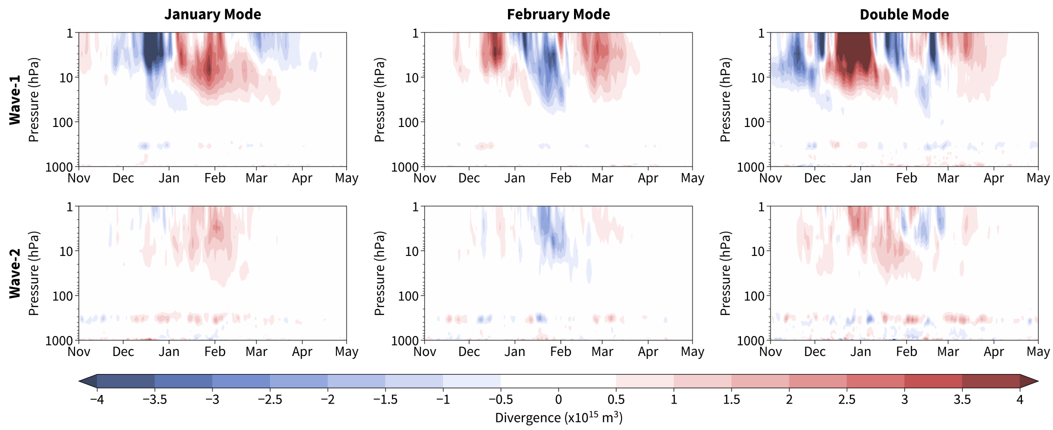

Figure A1. Contributions from Wave-1 and Wave-2 in the mean time-height development of the anomaly of the mass weighted divergence of Eliassen-Palm flux in the latitude range 50-70°N for the three perturbed scenarios. Shaded negative (blue) and positive (red) values correspond to a deceleration and acceleration of the zonal wind, respectively.

- In February and March, a positive AO phase is observed, accompanied by a positive geopotential anomaly concentrated in Western Europe. In March, this surface pattern is associated with temperature anomalies exceeding +3 K over the Barent Sea region, and on average, +1.5 K over East Siberia. Negative anomalies of -1.5 K, on average, are found over North-East America.

5. RFW mode:
   - Negative stratospheric anomaly descents occur from January to April during this mode. In January, a positive AO-like phase pattern is observed.
   - From February to March, a wave-2-like pattern emerges with positive geopotential anomalies over the U.S. West coast and western Europe, and negative anomalies over the Barent Sea region and Siberia's East coast.
   - Finally, in April, a pronounced positive phase of the AO emerges when the polar vortex disappears.

These findings significantly contribute to our understanding of stratosphere-troposphere coupling during the winter in the northern hemisphere, with important implications for sub-seasonal to seasonal climate forecasts. Future research should employ mechanistic models to test whether these precursors and specific wave activities associated with each scenario can simulate ISSWs with the expected timing. Furthermore, investigating the causes of stratospheric anomaly entry into the troposphere would be beneficial. Additional investigations are necessary to better comprehend the triggers for each scenario, with one potential avenue being to explore links with sea ice concentrations and thicknesses at the beginning of winter.

Appendix A Contributions from Wave-1 and Wave-2 in the divergence of Eliassen-Palm flux

Acknowledgments

This work was performed within the framework of the European ARISE project and was funded by the French Educational Ministry with EUR IPSL. Copernicus Climate Change Service (C3S): ERA5: Fifth generation of ECMWF atmospheric reanalyses of the global

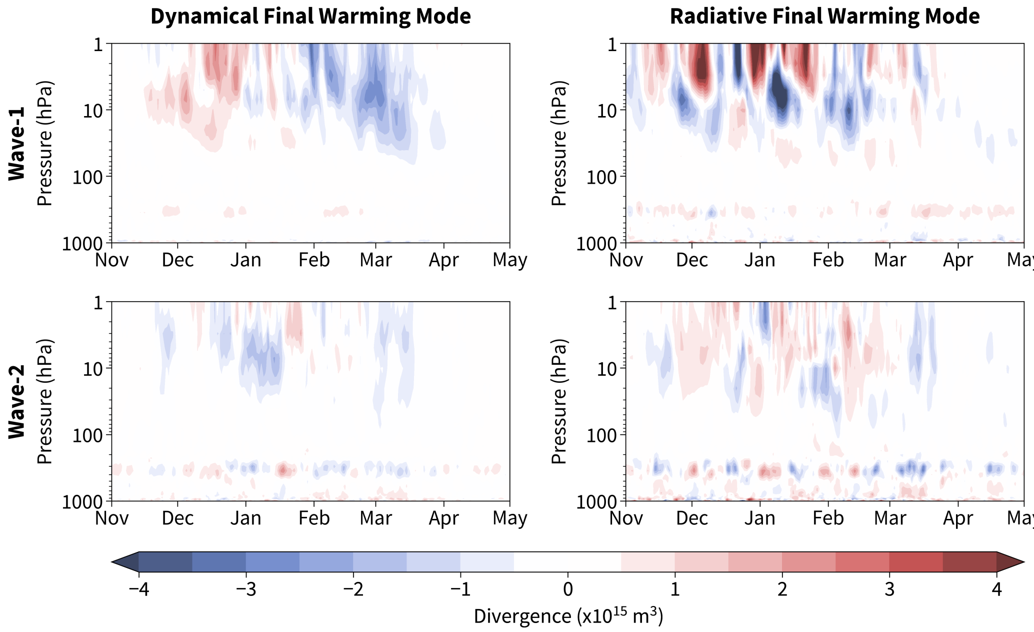

Figure A2. Contributions from Wave-1 and Wave-2 in the mean time-height development of the anomaly of the mass weighted divergence of Eliassen-Palm flux in the latitude range 50-70°N for the two sub-modes composing the unperturbed scenario. Shaded negative (blue) and positive (red) values correspond to a deceleration and acceleration of the zonal wind, respectively.

climate. Copernicus Climate Change Service Climate Data Store (CDS), accessible at: `https://cds.climate.copernicus.eu/cdsapp#!/home`.

References

Afargan-Gerstman, H., & Domeisen, D. I. V. (2020). Pacific modulation of the north atlantic storm track response to sudden stratospheric warming events. *Geophysical Research Letters*, *47*(2), e2019GL085007. doi: https://doi.org/10.1029/2019GL085007

Andrews, D. G., Mahlman, J. D., & Sinclair, R. W. (1983). Eliassen-palm diagnostics of wave-mean flow interaction in the gfdl "skyhi" general circulation model. *Journal of Atmospheric Sciences*, *40*(12), 2768 - 2784. doi: https://doi.org/10.1175/1520-0469(1983)040⟨2768:ETWATM⟩2.0.CO;2

Ayarzagüena, B., Langematz, U., & Serrano, E. (2011). Tropospheric forcing of the stratosphere: A comparative study of the two different major stratospheric warmings in 2009 and 2010. *Journal of Geophysical Research: Atmospheres*, *116*(D18). doi: https://doi.org/10.1029/2010JD015023

Baldwin, M. P., & Dunkerton, T. J. (2001). Stratospheric harbingers of anomalous weather regimes. *Science*, *294*(5542), 581-584. doi: 10.1126/science.1063315

Baldwin, M. P., & Thompson, D. W. (2009). A critical comparison of stratosphere–troposphere coupling indices. *Quarterly Journal of the Royal Meteorological Society*, *135*(644), 1661-1672. doi: https://doi.org/10.1002/qj.479

Bancalá, S., Krüger, K., & Giorgetta, M. (2012). The preconditioning of major sudden stratospheric warmings. *Journal of Geophysical Research: Atmospheres*, *117*(D4). doi: https://doi.org/10.1029/2011JD016769

Barriopedro, D., & Calvo, N. (2014). On the relationship between enso, stratospheric sudden warmings, and blocking. *Journal of Climate*, *27*(12), 4704 - 4720. doi: https://doi.org/

10.1175/JCLI-D-13-00770.1

Butler, A. H., & Domeisen, D. I. V. (2021). The wave geometry of final stratospheric warming events. *Weather and Climate Dynamics*, *2*(2), 453–474. doi: 10.5194/wcd-2-453-2021

Butler, A. H., Seidel, D. J., Hardiman, S. C., Butchart, N., Birner, T., & Match, A. (2015). Defining sudden stratospheric warmings. *Bulletin of the American Meteorological Society*, *96*(11), 1913 - 1928. doi: https://doi.org/10.1175/BAMS-D-13-00173.1

Charlton, A. J., & Polvani, L. M. (2007). A new look at stratospheric sudden warmings. part i: Climatology and modeling benchmarks. *Journal of Climate*, *20*(3), 449 - 469. doi: https://doi.org/10.1175/JCLI3996.1

Cohen, J., & Jones, J. (2011). Tropospheric precursors and stratospheric warmings. *Journal of Climate*, *24*(24), 6562 - 6572. doi: https://doi.org/10.1175/2011JCLI4160.1

Domeisen, D. I. (2019). Estimating the frequency of sudden stratospheric warming events from surface observations of the north atlantic oscillation. *Journal of Geophysical Research: Atmospheres*, *124*(6), 3180-3194. doi: https://doi.org/10.1029/2018JD030077

Edmon, H. J., Hoskins, B. J., & McIntyre, M. E. (1980). Eliassen-palm cross sections for the troposphere. *Journal of Atmospheric Sciences*, *37*(12), 2600 - 2616. doi: https://doi.org/10.1175/1520-0469(1980)037⟨2600:EPCSFT⟩2.0.CO;2

Esler, J. G., & Scott, R. K. (2005). Excitation of transient rossby waves on the stratospheric polar vortex and the barotropic sudden warming. *Journal of the Atmospheric Sciences*, *62*(10), 3661 - 3682. doi: https://doi.org/10.1175/JAS3557.1

Hauchecorne, A., Claud, C., Keckhut, P., & Mariaccia, A. (2022). Stratospheric final warmings fall into two categories with different evolution over the course of the year. *Communications Earth & Environment*, *3*(1), 4. doi: https://doi.org/10.1038/s43247-021-00335-z

Hersbach, H., Bell, B., Berrisford, P., Hirahara, S., Horányi, A., Muñoz-Sabater, J., ... Thépaut, J.-N. (2020). The era5 global reanalysis. *Quarterly Journal of the Royal Meteorological Society*, *146*(730), 1999-2049. doi: https://doi.org/10.1002/qj.3803

Jucker, M. (2021). Scaling of eliassen-palm flux vectors. *Atmospheric Science Letters*, *22*(4), e1020. doi: https://doi.org/10.1002/asl.1020

Karpechko, A. Y., Hitchcock, P., Peters, D. H. W., & Schneidereit, A. (2017). Predictability of downward propagation of major sudden stratospheric warmings. *Quarterly Journal of the Royal Meteorological Society*, *143*(704), 1459-1470. doi: https://doi.org/10.1002/qj.3017

Kidston, J., Scaife, A. A., Hardiman, S. C., Mitchell, D. M., Butchart, N., Baldwin, M. P., & Gray, L. J. (2015). Stratospheric influence on tropospheric jet streams, storm tracks and surface weather. *Nature Geoscience*, *8*(6), 433–440. doi: https://doi.org/10.1038/ngeo2424

Kodera, K., Funatsu, B. M., Claud, C., & Eguchi, N. (2015). The role of convective overshooting clouds in tropical stratosphere–troposphere dynamical coupling. *Atmospheric Chemistry and Physics*, *15*(12), 6767–6774. doi: 10.5194/acp-15-6767-2015

Kodera, K., Mukougawa, H., Maury, P., Ueda, M., & Claud, C. (2016). Absorbing and reflecting sudden stratospheric warming events and their relationship with tropospheric circulation. *Journal of Geophysical Research: Atmospheres*, *121*(1), 80-94. doi: https://doi.org/10.1002/2015JD023359

Mariaccia, A., Keckhut, P., & Hauchecorne, A. (2022). Classification of stratosphere winter evolutions into four different scenarios in the northern hemisphere. *Journal of Geophysical Research: Atmospheres*, *127*(13), e2022JD036662. doi: https://doi.org/10.1029/2022JD036662

Mariaccia, A., Keckhut, P., Hauchecorne, A., Claud, C., Le Pichon, A., Meftah, M., & Khaykin, S. (2022). Assessment of era-5 temperature variability in the middle atmosphere using rayleigh lidar measurements between 2005 and 2020. *Atmosphere*, *13*(2). doi: 10.3390/atmos13020242

Marlton, G., Charlton-Perez, A., Harrison, G., Polichtchouk, I., Hauchecorne, A., Keckhut, P., ... Steinbrecht, W. (2021). Using a network of temperature lidars to identify temperature biases in the upper stratosphere in ecmwf reanalyses. *Atmospheric Chemistry and Physics*, *21*(8), 6079–6092. doi: 10.5194/acp-21-6079-2021

Matsuno, T. (1970). Vertical propagation of stationary planetary waves in the winter northern hemisphere. *Journal of Atmospheric Sciences*, *27*(6), 871 - 883. doi: https://doi.org/10.1175/1520-0469(1970)027⟨0871:VPOSPW⟩2.0.CO;2

Mitchell, D. M., Gray, L. J., Anstey, J., Baldwin, M. P., & Charlton-Perez, A. J. (2013). The influence of stratospheric vortex displacements and splits on surface climate. *Journal of Climate*, *26*(8), 2668 - 2682. doi: https://doi.org/10.1175/JCLI-D-12-00030.1

Nakagawa, K. I., & Yamazaki, K. (2006). What kind of stratospheric sudden warming propagates to the troposphere? *Geophysical Research Letters*, *33*(4). doi: https://doi.org/10.1029/2005GL024784

Runde, T., Dameris, M., Garny, H., & Kinnison, D. E. (2016). Classification of stratospheric extreme events according to their downward propagation to the troposphere. *Geophysical Research Letters*, *43*(12), 6665-6672. doi: https://doi.org/10.1002/2016GL069569

Thompson, D. W. J., & Wallace, J. M. (2001). Regional climate impacts of the northern hemisphere annular mode. *Science*, *293*(5527), 85-89. doi: 10.1126/science.1058958

Tripathi, O. P., Baldwin, M., Charlton-Perez, A., Charron, M., Eckermann, S. D., Gerber, E., ... Son, S.-W. (2015). The predictability of the extratropical stratosphere on monthly time-scales and its impact on the skill of tropospheric forecasts. *Quarterly Journal of the Royal Meteorological Society*, *141*(689), 987-1003. doi: https://doi.org/10.1002/qj.2432

Vargin, P., Luk'yanov, A., & Kiryushov, B. (2020). Dynamic processes in the arctic stratosphere in the winter of 2018/2019. *Russian Meteorology and Hydrology*, *45*, 387–397. doi: https://doi.org/10.3103/S1068373920060011

Waugh, D. W., & Rong, P.-P. (2002). Interannual variability in the decay of lower stratospheric arctic vortices. *Journal of the Meteorological Society of Japan. Ser. II*, *80*(4B), 997–1012. doi: https://doi.org/10.2151/jmsj.80.997